Dear Dr. Langebroek,

Thanks for the constructive comments. The manuscript has been clarified and improved by taking your comments into account.

Notes: unless otherwise specified, line numbers refer to the non-updated manuscript version. The authors' comments are in blue, and the changes in the manuscript are in green.

General Comments

1. More discussion is needed on section 2 Antarctic ice-sheet geometry. There is a nice overview of literature, but no discussion on why the ice sheet configurations of the previous Miocene studies are discarded, and why Pollard's Oligocene configuration was used instead. You probably prefer to not use the configurations of Langebroek and Oerlemans, as they use rather simple model configurations. But why do you discard the geometry of Gasson et al.? Related: what forcing and boundary conditions are used in Pollard's simulations? How does that compare to the Middle Miocene?

As the reviewer mentions, the reason why Oerlemans and Langebroek's configurations were discarded is that they use rather simple model configurations. We wanted to provide a characterization of the Antarctic ice-sheet in two dimensions, i.e. varying with both latitude and longitude, and this is not available from Oerlemans or Langebroek's studies.
The scope of the current study was to provide Antarctic topography data consistent with published Antarctic ice volume estimates for the MMCO and MMG, and this was successfully accomplished. The configuration of Gasson et al. (2016) could be considered in future sensitivity studies, because uncertainties in the ice-volume estimates are high, but we consider the data from Pollard's simulations used here definitely suitable for the Middle Miocene since there is little to link those data to a specific time period (except for the Laskar orbits) (see below). Additionally, the distribution of ice in our study is comparable to that in Gasson et al. (2016): for the MMG, a continental scale ice-sheet exists in East Antarctica with ice

thicknesses of ~3000-4000 m, although in West Antarctica there is less ice in Pollard's data; for the MMCO, the ice-sheets occupy similar positions, although they are less extensive in Pollard's data.

Regarding David Pollard's simulations, the physical model used is close to that described in Pollard and DeConto (2012), but with no marine ice physics, so that any floating ice is immediately removed. The bedrock-elevation boundary conditions are from the modern ALBMAPv1 dataset (Le Brocq et al., 2010).

Climate forcing is obtained from a matrix of previous Global Climate Model (GCM) climates for various orbits, CO2 levels and ice sizes. The GCM used is GENESIS version 3 (as in Alder et al., 2011, except with a slab mixed layer ocean). Three Earth orbits are used, with eccentricity, precession and obliquity set corresponding to warm, intermediate and cold austral summers. Three CO2 levels are used, spanning the range in the long term run. Three Antarctic ice sizes (continental, ~half and no ice cover) are specified. 10-year mean equilibrated GCM climate solutions (i.e., monthly mean surface air temperatures and precipitation) are saved for all combinations of orbit, CO2 and ice size, yielding a matrix of 27 climates.

In the long-term ice-sheet run, the appropriate climate at any point in the run is obtained by linearly weighting the surrounding saved climates in the matrix, with the weights proportional to the current austral summer insolation, ice size and logarithm of CO2 level. This matrix-forcing method is discussed further in Pollard (2010). The annual surface mass balance at each point on the ice sheet is calculated from the monthly surface air temperatures and precipitation, using a simple box (zero-dimensional) seasonal surface-mass model that includes snow storage and refreezing of meltwater, and surface melting based on Positive Degree Days (Pollard and DeConto, 2012). The run is initialized with (essentially) no ice. Insolation is based on Laskar et al. (2004). The run is 12 Myr long, nominally from "37 Ma to 25 Ma", although there is little to actually link it to specific paleodates except the Laskar orbits. From 37 to 33 Ma, CO2 decreases linearly from 6xPAL to 2xPAL. From 33 to 25 Ma, CO2 increases linearly from 2xPAL to 10xPAL (where PAL= 280 ppmv). The configuration used to represent MMCO conditions corresponds to 34.8 Ma (CO2 = 3.8xPAL). The one representing MMG conditions, to 33 Ma (CO2 = 2xPAL).

Lines 82-99 (old numeration) have been rewritten.

2. Section 4 describing the different published atmospheric CO2 levels is somewhat difficult to follow. A figure showing all the different published records over the Middle Miocene, in combination with horizontal lines indicating your suggestion, would clarify this section. Additionally a discussion on why these values are all so different is needed.

The reviewer's suggestion is interesting, although we do not see the addition of a figure as a requirement for the comprehension of the CO2 section. Nevertheless, lines 162-168 (now lines 205-214) have been rephrased as follows to make the section more clear:

'We chose atmospheric CO_2 concentrations of 400 ppmv and 200 ppmv to represent the MMCO and the MMG respectively (Table 1). Although somewhat arbitrary, these values are within the range of published estimates. The 400 ppmv MMCO is in favourable agreement with Foster et al. (2012) (~392 ppmv at ~15.8 Ma) and Tripati et al. (2009) (~430 ppmv at ~15.1 Ma), although higher than Pearson et al. (2000) (~300 ppmv at ~16.2 Ma) and Pagani et al. (2005) (~300 ppmv at ~15 Ma), and lower than Kürschner et al. (2008) (> ~400-500 ppmv at ~15.5 Ma) and Retallack (2009) (~852 ppmv at ~15.6 Ma) maxima. The 400 ppmv estimate is also in good agreement with the most recent alkenone- and boron isotope-based pCO2 reconstructions for the MMCO by Zhang et al. (2013) and Greenop et al. (2014). The 200 ppmv MMG estimate is in good agreement with Foster et al. (2012) (~200 ppmv at ~12 Ma) and Pagani et al. (2005) (~200 ppmv at ~13 Ma), although higher than Pearson et al. (2000) (~140 ppmv at ~14.7 Ma) and Retallack (2009) (~116 ppmv at ~14.6 Ma), and lower than Tripati et al. (2009) (~340 ppmv at ~12 Ma) and Kürschner et al. (2008) (~280 ppmv at ~14 Ma) minima.'

The difference in the CO_2 estimates between the various studies arises most likely from method-related uncertainties and/or the relatively coarse temporal resolution of some of the datasets.

We added a note at line 185 (new numeration):
'The difference in the CO_2 estimates between the various studies arises most likely from method-related uncertainties and/or the relatively coarse temporal resolution of some of the datasets'.

3. Section 5.3, especially lines 204-214 are too detailed. Please make this section more concise. Maybe "We used ArcGIS to convert ... to ..."

The text at lines 204-214 (old numeration) has been shortened:
'South East Asian paleogeography was modified based on Hall's (2012) reconstruction constrained at 15 Ma (Fig. 3). Hall's data, available as a georeferenced image, were converted into grid format using ArcGIS. Qualitative height/depth values were assigned to the different geographic features: ~2800 m for volcanoes, ~1000 m for highlands, ~250 m for land, ~-22 m for carbonate platforms, ~-200 m for shallow sea, <-4000 m for deep sea, and ~-5500 m for trenches. After embedding the data into the MMCO global dataset, minor manual smoothing was applied at the margins of the embedded region. Here, shallow bays were removed and single, shallow grid points surrounded by much deeper grid points were deepened to the adjacent depth. In total, these modifications affected ~0.5% of the total number of grid points.'

4. Concerning the global topography/bathymetry section: a difference plot to the Herold et al reconstruction (or at least additional information on this) would be highly relevant.

A new figure has been added (and a reference to it at line 243 (new numeration)).

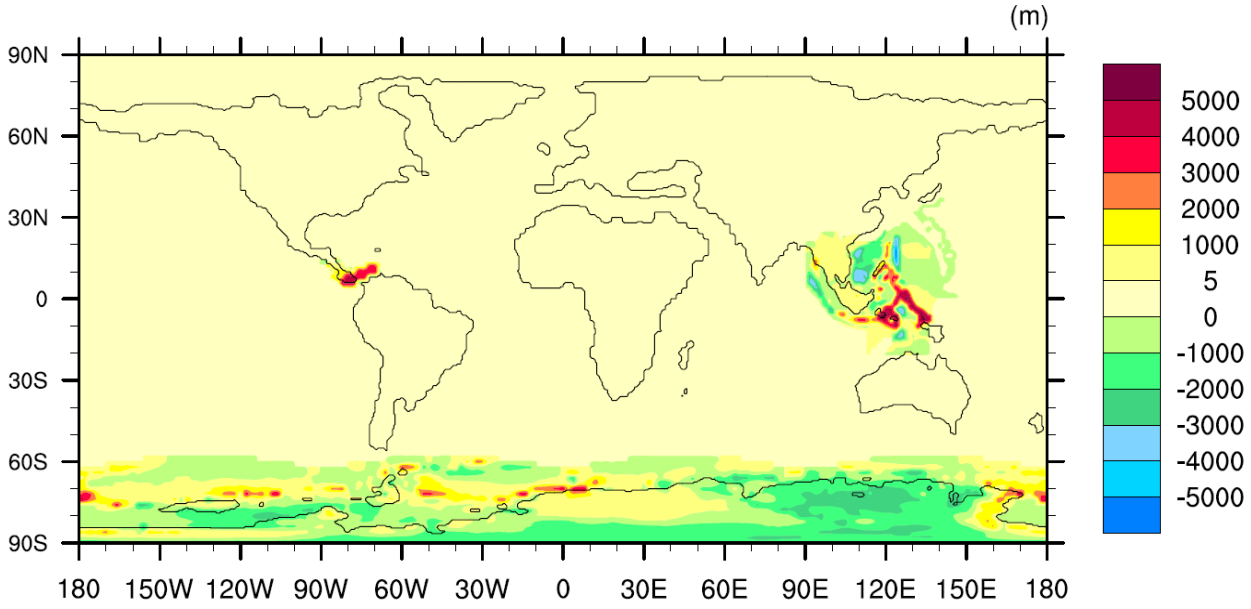

Figure S1: Difference between MMCO and the topography/bathymetry by Herold et al. (2008), in meters. Sea level is 4 m higher in the MMCO dataset (subsection 5.2), the Indonesian Throughflow barriers are shallower (subsection 5.3), the Panama seaway is narrower (subsection 5.4), and the Antarctic topography/bathymetry is based on David Pollard's data (subsection 5.1) and consistent with MMCO ice volume estimates.

5. Now my biggest concern: The description of the vegetation (Section 6). This section is very lengthily, and to be honest not very useful. In many subsections the vegetation patterns from literature are stated, but then subsequently ignored because you prefer to have a low resolution, simple, distribution. I have no problem with the latter, but I then do not see the use of discussing in detail the vegetation in each continent. I also do see that vegetation might be an important boundary condition, and suggest applying an offline vegetation model (e.g. BIOME4) in order to get a more consistent vegetation pattern within your model set-up. This could then be compared and discussed with previous studies, also previous modelling studies (for example Bradshaw et al., 2012).

Although a detailed discussion on the vegetation of each region is not indispensable for the comprehension of this manuscript, we think that it is important to show how exactly we decided what vegetation to assign to each region.

Subsections 6.1-6.9 have thus been moved to the Appendix (Sect. 10), in case the reader was interested in those details. A reference to the Appendix has been added at line 360 (new numeration).

The reviewer's suggestion of using the output from an offline vegetation model as a boundary condition is very interesting (e.g., the ones described in Henrot et al., 2017), although here our aim was to provide boundary conditions based on palaeobotanical data. The vegetation output from an offline vegetation model is based on a climatic forcing. In our study the approach was the opposite: using vegetation data to be able to produce a climatic output. An alternative for GCMs including a dynamic vegetation component would be to use our Middle Miocene vegetation dataset to initialize the vegetation model. Nevertheless, we consider that, although coarse, our dataset provides a fair characterization of Middle Miocene global vegetation patterns.

A note has been added at line 355 (new numeration).

6. The final part, the model simulations, are interesting, but need discussion:

a. How is the grid extended to reach higher southern latitudes? Does this mean that the resolution is lower in the Miocene simulations compared to the PI simulation? How do you make difference plots then (regridding?)? Does this have an impact on the results?

The Miocene grid is a dipole grid created from scratch using the CCSM3 setup tools described in Rosenbloom et al. (2011) and defined by the following parameters: dyeq=0.25 (meridional grid spacing at the equator, in degrees), dsig=20 (Gaussian e-folding scale at equator), and jcon=45 (rows of constant meridional grid spacing at poles).
In some areas the Miocene grid presents a slightly coarser resolution than the PI grid, since both grids have the same number of grid points (384x320) and the Miocene grid reaches further south than the PI grid (~87°S vs ~79°S).
Difference plots are made by regridding from the PI grid onto the Miocene grid. The method used is the "patch recovery" method (http://www.ncl.ucar.edu/Applications/ESMF.shtml), which gives better approximations than the "bilinear" method. We do not think interpolation has any significant effect on the results.

The reviewer's comment has been addressed in the manuscript at lines 549-556 (new numeration).

b. Are the simulations run long enough? What are the trends in the deep ocean (temperatures, salinity, …)?

The temperature trends in the deep ocean (at 4-5 km depth) are < 0.14, 0.15, and 0.17 °C/100 years in the PI, MMCO, and MMG cases, respectively. At that same depth range, the salinity trends are <0.01, 0.007, and 0.01 psu/100 years for PI, MMCO, and MMG, respectively. These values represent quasi-equilibrium conditions and we consider them sufficiently small for the focus of this study.

The reviewer's comment has been addressed in the manuscript at lines 565-568 (new numeration).

c. The comparison of the precipitation needs to be rewritten. The lower/higher precipitation along the coast of South America seems to be due to the movement of the continents. Maybe more interesting would be to discuss the apparent shift in the ITCZ. Why?

We checked again the absolute precipitation maps (see Figure S2) and the Miocene experiments present lower precipitation rates than PI along the northwest coast of South America. Nevertheless, the difference of 5-6 mm/day we suggested is too high, and as the reviewer noted, linked to the movement of the continents.

The text has been modified by replacing 'up to 5-6 mm/day lower' with '3-4 mm/day lower' at line 572 (new numeration). We also added a paragraph on the ITCZ. Please, check lines 575-579 (new numeration) for more details. Additionally, a new figure (Fig. S2) has been added (please, see below).

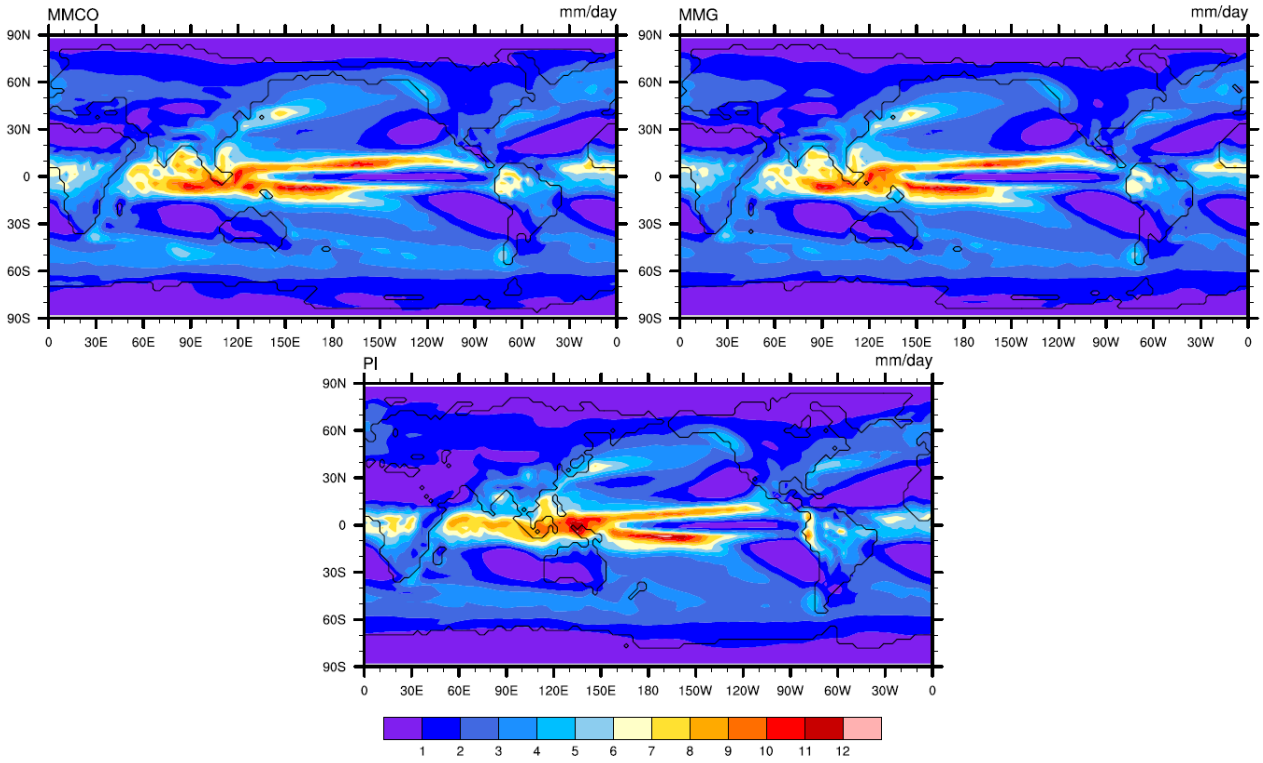

Figure S2: Precipitation for MMCO, MMG, and PI, in mm/day.

d. Also the temperature comparison lacks discussion. Why is the MMG simulation warmer than PI? CO2 is lower (200 ppm), right? How different is the Antarctic ice sheet compared to today? Is the cooling in the Pacific caused by changes in gateways/geography/topography? Please discuss.

Indeed, CO2 is lower in the MMG simulation than in the control run (MMG: CO2 = 200 ppmv, PI: CO2 = 280 ppmv). Nevertheless, SST's are higher for MMG (18.04°C) than for PI (16.85°C). Potential causes for a MMG climate warmer than PI could be the lower extent of ice-sheets (the Antarctic ice-sheet is smaller and the northern Hemisphere free of ice-sheets in the MMG run), or the different vegetation cover (Knorr et al., 2011). However, unambiguously disentangling the effects of each of the different boundary conditions would require performing a series of sensitivity experiments, which was beyond the scope of the current study. Here our aim was testing the idoneity of the current boundary conditions as input data in GCMs for MMCO and MMG experiments.

In the MMG experiment the Antarctic ice-sheet has a volume of 23 million km³, hence lower than present-day (27 million km³, according to Fretwell et al., 2013).

This point has been addressed at lines 592-598 (new numeration).

e. During this discussion please list again the differences between the Miocene simulations (400 vs 200 ppm; different Antarctic ice sheet and vegetation). What is the climate sensitivity of this model? A 200 ppm decrease in CO2 would cause a reduction in temperature of about 2-4°C? Why is there only a difference of 1.6°C? Is the difference larger when you take the global mean surface air temperature? And how much of the cooling is due to the ice expansion (and related albedo changes)? Please discuss.

The climate sensitivity of CCSM3 is discussed in Kiehl et al. (2006), where two different approaches are used, one based on results from a slab ocean run with fixed CO2 and the other one based on a fully coupled run with increasing CO2 rates. The results obtained are 2.47°C and 1.48°C, respectively.
When, instead of SSTs, surface air temperatures (at 2 m height) are considered, our results show mean global values of 16.38°C, 13.88°C, and 12.16°C for the MMCO, MMG, and PI, respectively. This implies a decrease of 2.5°C between the MMCO (CO2= 400 ppmv + small Antarctic ice-sheet) and MMG (CO2= 200 ppmv + expanded ice-sheet), which is in good agreement with the CCSM3 climate sensitivity values suggested in Kiehl et al. (2006). A decrease of 1.6°C in SST's would also be in agreement with Kiehl et al. (2006).
Quantifying how much of the cooling is due to ice expansion is a very interesting suggestion, although it would require performing a series of sensitivity studies, with fixed CO2 and varying Antarctice ice volume, which were beyond the scope of the current study. Here our aim was testing the idoneity of the current boundary conditions as input data in GCMs for MMCO and MMG experiments.

The reviewer's comment has been addressed at lines 584-588 (new numeration).

Specific Comments

1. The start of Section 3 is somewhat confusion, because of the connection between Antarctic ice volume (defined for the Middle Miocene at the end of Section 2) and sea level. Maybe it would be better to start Section 3 with lines 132-136, followed by the discussion of other literature values.

Lines 132-136 have been moved to the top of the section. However, those lines have been slightly rephrased because they contained a reference to Equation (1), which had not been defined yet.

Lines 112-118 were removed because they had become redundant.

2. Why is the topography over Greenland so high in the Middle Miocene? It looks much higher than a present-day isostatically rebounded topography.

Our values are based on Herold et al. (2008). In that study, the topography over Greenland is "reduced by 2300 m" compared to present-day and "isostatically corrected by 1651 m", which means that it is 649 m lower than at present-day. We compared our topography to Bamber et al. (2001) present-day isostatically rebounded topography (Figure 5 in Bamber et al., 2001). We agree with the reviewer that our topography is a bit higher, reaching maximum values of ~2400 m, versus maximum values of ~2000 m in Bamber et al. (2001). Nevertheless, we believe that Herold's values are still a good approximation of an ice-free Greenland topography.

Technical Comments

-Line 12: add "successfully" to applied.

Added.

-Lines 20-21: rewrite. δ18O could also reflect a combined change in ice volume and temperature.

We added this text:
'or a combination of both'.

-Line 25: change "would have been" to "were".

Changed.

-Line 28: explain "important".

A reference to Section 3 has been added. In this section, sea level fall published estimates for the Middle Miocene Climate Transition are reviewed in detail.

-Line 40: add "e.g." before references. Using an intermediate complexity climate and ice sheet model, Langebroek et al. (2010) showed that a combination of pCO2 decrease and orbital forcing causes an Antarctic ice sheet expansion that can explain the majority of the benthic δ18O increase.

Added at line 47(new numeration), although slightly rephrased:
'Langebroek et al. (2010), for example, using an isotope enabled ice-sheet–climate model forced with a pCO2 decrease and varying time-dependent orbital parameters, modeled an increase in δ18O of sea water in good agreement with published MMCT estimates.'

-Line 54: change "data" to "boundary conditions".

Changed.

-Line 61: change "studies" to "sediment core data".

'Studies' has been replaced with 'sediment core studies'.

-Line 67: change "simulations" to "study".

Changed (now line 77).

-Line 93: "This estimate" instead of "This 6 estimate".

Done (now line 95).

-Line 104: change "very few" to "little".

Changed.

-Line 190: change "Some" to "Additional". And make clear in this sentence that the modifications will be discussed below.

Done.

A comment has been added at line 191 (now line 243):
'(see discussion below in subsections 5.1–5.4)'.

-Line 198: "64" where does this number come from?

The 64 m present-day sea-level equivalent value is in good agreement with Vaughan et al. (2013) (58.3 m for the Antarctic ice-sheet and 7.36 m for the Greenland ice-sheet).

The following text has been added at line 251 (new numeration):
'This present-day estimate is in good agreement with Vaughan et al. (2013) (58.3 m for the Antarctic ice-sheet and 7.36 m for the Greenland ice-sheet).'

-Line 448: what does "T42x1" mean? Especially the "x1"?

T42 is the atmosphere horizontal grid, a Gaussian grid with 64 points in latitude and 128 points in longitude (~2.8° resolution). The notation T42 refers to the spectral truncation level. x1 is the ocean horizontal grid, a dipole grid with 384 points in latitude and 320 points in longitude. The zonal resolution of the ocean horizontal grid is ~1°, the mean meridional resolution is ~0.5°, refined around the equator (~0.3°). The notation x1 refers to the nominal zonal resolution. T42x1 is the model configuration employing the T42 and x1 grids.

Lines 448-453 (old numeration) have been modified as follows:
'The atmosphere horizontal grid employed in the PI run, T42, is a Gaussian grid with 64 points in latitude and 128 points in longitude (~2.8° resolution). The notation T42 refers to the spectral truncation level. The land and atmosphere models share the same horizontal grid. The ocean horizontal grid, x1, is a dipole grid with 384 points in latitude and 320 points in longitude. The zonal resolution of the ocean horizontal grid is ~1°, the mean meridional resolution is ~0.5°, refined around the equator (~0.3°). The notation x1 refers to the nominal zonal resolution. The ocean and sea–ice components share the

same horizontal grid. The atmosphere and ocean vertical grids have 26 and 40 vertical levels, respectively. This model grid configuration is known as T42x1.'

-Line 459: rephrase to "were set to PI following Otto-Bliesner".

Rephrased.

-Line 471: change "observed" to "simulated".

The word "observed" does not appear in the text anymore. We rewrote that part of the text in relation to the reviewer's comment: 6 c).

-Line 477: change "complete compilation" to "complete set".

Changed.

-Line 481: change "treated" to "discussed".

Changed.

-Figure 1: caption: change "total elevation" to surface elevation". Colours: The colour scale is not great. By colouring 0 to -1000 white, it seems to belong to land, while it is actually ocean. Please change this. Also ice thickness cannot be negative, please update colour bar.

Done.

-Figure 4: Please make the order of the abbreviations in the caption consistent with the order in the colour bar.

Done.

Additional modifications:

-Line 73 (now line 83):

In Langebroek et al. (2010) the model is isotope-enabled, but in Langebroek et al. (2009) it is not.

We have thus rephased 'Langebroek et al. (2009) used a coupled isotope-enabled ice-sheet–climate model' as 'Langebroek et al. (2009) used a coupled ice-sheet–climate model'.

We hope we have addressed all your comments.

Yours sincerely,

Amanda Frigola and co-authors.

References:

Alder, J. R., Hostetler, S. W., Pollard, D., and Schmittner, A.: Evaluation of a present-day climate simulation with a new coupled atmosphere-ocean model GENMOM, GMD, 4(1), 69–83, doi:10.5194/gmd-4-69-2011, 2011.

Bamber, J. L., Layberry, R. L., and Gogineni, S. P.: A new ice thickness and bed data set for the Greenland ice sheet 1. Measurement, data reduction, and errors, J. Geophys. Res.-Atmos., 106(D24), 33773-33780, doi:10.1029/2001JD900054, 2001.

Fretwell, P., Pritchard, H. D., Vaughan, D. G., Bamber, J. L., Barrand, N. E., Bell, R., Bianchi, C., et al.: Bedmap2: improved ice bed, surface and thickness datasets for Antarctica, Cryosphere, 7, 375–393, doi:10.5194/tc-7-375-2013, 2013.

Gasson, E., DeConto, R. M., Pollard, D. and Levy, R. H.: Dynamic Antarctic ice sheet during the early to mid-Miocene, P. Natl. Acad. Sci., 113(13), 3459–3464, doi:10.1073/pnas.1516130113, 2016.

Groeneveld, J., Henderiks, J., Renema, W., McHugh, C. M., De Vleeschouwer, D., Christensen, B. A., Fulthorpe, C. S., Reuning, L., Gallagher, S. J., Bogus, K., Auer, G., Ishiwa, T., and Expedition 356 Scientists: Australian shelf sediments reveal shifts in Miocene Southern Hemisphere westerlies, Sci. Adv., 3(5), 1–9, doi:10.1126/sciadv.1602567, 2017.

Henrot, A.-J., Utescher, T., Erdei, B., Dury, M., Hamon, N., Ramstein, G., Krapp, M., Herold, N., Goldner, A., Favre, E., Munhoven, G., and François, L.: Middle Miocene climate and vegetation models and their validation with proxy data, Palaeogeogr. Palaeoclimatol. Palaeoecol., 467, 95–119, doi:10.1016/j.palaeo.2016.05.026, 2017.

Herold, N., Seton, M., Müller, R. D., You, Y. and Huber, M.: Middle Miocene tectonic boundary conditions for use in climate models, Geochem. Geophy. Geosy., 9(10), Q10009, doi:10.1029/2008GC002046, 2008.

Holbourn, A., Kuhnt, W., Regenberg, M., Schulz, M., Mix, A., and Andersen, N.: Does Antarctic glaciation force migration of the tropical rain belt?, Geology, 38(9), 783–786, doi:10.1130/G31043.1, 2010.

Kiehl, J. T., Shields, C. A., Hack, J. J., Collins, W. D.: The Climate Sensitivity of the Community Climate System Model Version 3 (CCSM3), J. Climate, 19, 2584–2596, doi:10.1175/JCLI3747.1, 2006.

Knorr, G., Butzin, M., Micheels, A., and Lohmann, G.: A warm Miocene climate at low atmospheric CO2 levels, Geophys. Res. Lett., 38, L20701, 1–5, doi:10.1029/2011GL048873, 2011.

Langebroek, P. M., Paul, A. and Schulz, M.: Antarctic ice-sheet response to atmospheric CO2 and insolation in the Middle Miocene, Clim. Past, 5(4), 633–646, doi:10.5194/cp-5-633-2009, 2009.

Langebroek, P. M., Paul, A. and Schulz, M.: Simulating the sea level imprint on marine oxygen isotope records during the middle Miocene using an ice sheet-climate model, Paleoceanography, 25(4), PA4203, doi:10.1029/2008PA001704, 2010.

Laskar, J., Robutel, P., Joutel, F., Gastineau, M., Correia, A. C. M., Levrard, B.: A long term numerical solution for the insolation quantities of the Earth, 428, 261-285, A&A, doi:10.1051/0004-6361:20041335, 2004.

Le Brocq, A. M., Payne, A. J., and Vieli, A.: An improved Antarctic dataset for high resolution numerical ice sheet models (ALBMAP v1), Earth Syst. Sci. Data., 2 (2), 247-260, doi:10.5194/essd-2-247-2010, 2010.

Pollard, D.: A retrospective look at coupled ice sheet–climate modeling, Clim. Change, 100, 173-194, doi:10.1007/s10584-010-9830-9, 2010.

Pollard, D. and DeConto, R. M.: Description of a hybrid ice sheet-shelf model, and application to Antarctica, Geosci. Model Dev., 5, 1273-1295, doi:10.5194/gmd-5-1273-2012, 2012.

Rosenbloom, N., Shields, C., Brady, E., Levis, S. and Yeager, S.: Using CCSM3 for Paleoclimate Applications, NCAR Technical Note NCAR/TN–483+STR, National Center for Atmospheric Research, Boulder, Colorado, 1–81, doi:10.5065/D69S1P09, 2011.

Vaughan, D. G., Comiso, J. C., Allison, I., Carrasco, J., Kaser, G., Kwok, R., Mote, P., Murray, T., Paul, F., Ren, J., Rignot, E., Solomina, O., Steffen, K., and Zhang, T.: Observations: Cryosphere, in: Climate Change 2013: The Physical Science Basis. Contribution of Working Group I to the Fifth Assessment Report of the Intergovernmental Panel on Climate Change, edited by Stocker, T. F., Qin, D., Plattner, G. K., Tignor, M., Allen, S. K., Boschung, J., Nauels, A., Xia, Y., Bex, V., and Midgley, P. M., Cambridge University Press, Cambridge, United Kingdom and New York, NY, USA, 317-382, 2013.

Dear Dr. Henrot,

Thanks for the constructive comments. The manuscript has been clarified and improved by taking your comments into account.

Notes: unless otherwise specified, line numbers refer to the non-updated manuscript version. The authors' comments are in blue, and the changes in the manuscript are in green.

General comments:

1. Due to the scarcity of palaeovegetation records and the difficulties linked to the identification of plant taxa and correspondence to larger vegetation classes (Plant Functional Types (PFTs) or biomes), the reconstruction of a global vegetation distribution for the Miocene is certainly not easy and subject to many assumptions. Simple and static vegetation maps, mainly based on the reconstruction by Wolfe (1985) have been prescribed in previous modeling studies (Herold et al., 2010; Hamon et al., 2012; Goldner et al., 2014). In that way, deriving a global vegetation map from the reconstruction of Pound et al. (2012), based on the latest palaeovegetation data available, can improve the quality of the vegetation cover to be prescribed. However, the numerous simplifications in the biome classification applied here mask the improvements that could be added to the vegetation reconstruction. The authors end up with a very coarse vegetation distribution, with no differences, except tundra in Antarctica, between the two studied periods, and lack the potential feedback on climate of vegetation change. Wouldn't it be possible to directly interpolate the point-based vegetation reconstruction proposed by Pound et al. (2012) for the Langhian (representative of the MMCO) and for the Serravallian (representative of the MMG) to a 2° map, without so many simplifications, and to keep a maximum of the different biomes listed by Pound et al. (2012)?

Pound et al. (2012) dataset definitely constitutes an improvement in terms of the characterization of the Middle Miocene vegetation patterns. Nevertheless interpolation is problematic since some vast areas (e.g. Africa) present still low data coverage. Extrapolation is thus required. The difficulty arises in how to appropriately extrapolate the palaeobotanical information from isolated data points into the area surrounding them, i.e, in how to decide what exact area around those data points can be represented by that same vegetation pattern. Plus extrapolation of biomes is conceptually complicated: what is for example the appropriate biome that should be assigned to a grid point close to a "deciduous shrub land" and a "tropical broadleaf evergreen forest"? Wolfe and Morley performed that extrapolation in their studies, but Pound et al. (2012) did not. That is the reason why we often opted for using Wolfe and Morley's data in regions where Pound et al.'s dataset presented low coverage.

Corrections could be applied in function of more detailed regional information from Wolfe (1985) and Morley (2011). Then, a translation from BIOME4 to LSM biome classification could be done. However, the number of biome classes should not be too restricted in order to not loose the distinction between warm/cool and drier biomes, helping to better represent the transition to drier and cooler landscape in the Serravallian (MMG here). If this first option is not possible, I would suggest to extend the number of LSM biomes used here to better represent the vegetation changes between MMCO and MMG.

Please, see below our reply to the reviewer's comments to lines 263-273.

Deriving the vegetation cover from an off-line vegetation model simulation could also be an option to get a global and gridded vegetation map consistent with the model set-up. Previous modeling studies have already done so (Krapp and Junglaus, 2011; Henrot et al., 2017).

The reviewer's suggestion of using the output from an offline vegetation model as a boundary condition is very interesting (e.g., the ones described in Henrot et al., 2017), although here our aim was to provide boundary conditions based on palaeobotanical data. The vegetation output from an offline vegetation model is based on a climatic forcing. In our study the approach was the opposite: using vegetation data to be able to produce a climatic output. An alternative for GCMs including a dynamic vegetation component would be to use our Middle Miocene vegetation dataset to initialize the vegetation model. Nevertheless, we consider that, although coarse, our dataset provides a fair characterization of Middle Miocene global vegetation patterns.

A note has been added at line 355 (new numeration).

2. The last section of the paper, presenting CCSM3 simulations, is too short in comparison to previous sections describing the boundary conditions and lacks a discussion of the simulation results. Evaluating the reliability of the climate simulations would help to prove the suitability of the boundary conditions for Miocene climate modeling. What are the global surface air temperature and precipitation differences between the MMCO, MMG and PI runs? What are the impacts of the boundary conditions changes on the simulated climates? Sensitivity experiments testing separately the impact of boundary condition changes are not presented here, but would it be possible to distinguish or at least discuss the possible impacts of the different boundary condition changes on the simulated climate. The discussion would also benefit from a comparison with previous modeling studies, at least for the MMCO (and even with the same model, see Herold et al. (2010)), and/or with available proxy-data (e.g., for SSTs).

Please, see below our reply to the reviewer's comments to Section 7. However, a detailed model-model or even model-data comparison is beyond the scope of this paper and will be the subject of future studies.

Specific comments:

Introduction: the Introduction would benefit from some description of the climate state of the Middle Miocene, to highlight the differences between MMCO and MMG climate and between the boundary condition sets that will be presented later in the paper.

We have added a short description of the Middle Miocene climate and we have linked it to the Middle Miocene Climate Transition.

Lines 17-18 (now lines 17-21) have been rewritten:
'The Middle Miocene (ca. 16–11.6 Ma) was marked by important changes in global climate. The first stage of this time period, the Middle Miocene Climatic Optimum (MMCO), was characterized by warm conditions, comparable to those of the late Oligocene. Although global climate remained warmer than present-day during the whole Miocene (Pound et al., 2012), an important climate transition associated with major Antarctic ice-sheet expansion and global cooling took place between ~15 and 13 Ma, the so called Middle Miocene Climate Transition (MMCT).'

Lines 36-37: this effect should be taken into account in the vegetation cover reconstruction provided in Section 6.

Please, see below our reply to the reviewer's comments to Line 263-273.

Lines 43-45: please give the resolution of the boundary conditions and the format they are available in.

A reference to Section 9 (Data availability) has been added, also at the beginning of Section 5 (Global topography and bathymetry) (line 222, new numeration) and Section 6 (Global vegetation) (line 293, new numeration). Additionally, in Section 9, the format of the data has been explicited (line 617, new numeration). The resolution of the boundary condition datasets can also be found in Section 9.

Lines 52-53: the vegetation reconstruction proposed here is not exactly an update of Wolfe (1985). The sentence should be rephrased.

Done.

It has been rephrased as:

'Here, also Middle Miocene data (Pound et al., 2012; Morley, 2011) have been used'.

Section 2: a discussion explaining the use of a previous Antarctic topography corresponding to the Oligocene instead of previous published Middle Miocene topographies is needed in Section 2. Some precision could be given concerning the Oligocene configuration and how it is suitable for the Middle Miocene.

The reason why Oerlemans and Langebroek's Middle Miocene configurations were discarded is that they use rather simple model configurations. We wanted to provide a characterization of the Antarctic ice-sheet in two dimensions, i.e. varying with both latitude and longitude, and this is not available from Oerlemans or Langebroek's studies.

The scope of the current study was to provide Antarctic topography data consistent with published Antarctic ice volume estimates for the MMCO and MMG, and this was successfully accomplished. The configuration of Gasson et al. (2016) could be considered in future sensitivity studies, because uncertainties in the ice-volume estimates are high, but we consider the data from Pollard's simulations used here definitely suitable for the Middle Miocene since there is little to link those data to a specific time period (except for the Laskar orbits) (see below). Additionally, the distribution of ice in our study is comparable to that in Gasson et al. (2016): for the MMG, a continental-scale ice-sheet exists in East Antarctica with ice thicknesses of ~3000-4000 m, although in West Antarctica there is less ice in Pollard's data; for the MMCO, the ice-sheets occupy similar positions, although they are less extensive in Pollard's data.

Regarding David Pollard's simulations, the physical model used is close to that described in Pollard and DeConto (2012), but with no marine ice physics, so that any floating ice is immediately removed. The bedrock-elevation boundary conditions are from the modern ALBMAPv1 dataset (Le Brocq et al., 2010).

Climate forcing is obtained from a matrix of previous Global Climate Model (GCM) climates for various orbits, CO2 levels and ice sizes. The GCM used is GENESIS version 3 (as in Alder et al., 2011, except with a slab mixed layer ocean). Three Earth orbits are used, with eccentricity, precession and obliquity set corresponding to warm, intermediate and cold austral summers. Three CO2 levels are used, spanning the range in the long term run. Three Antarctic ice sizes (continental, ~half and no ice cover) are specified. 10-year mean equilibrated GCM climate solutions (i.e., monthly mean surface air temperatures and precipitation) are saved for all combinations of orbit, CO2 and ice size, yielding a matrix of 27 climates.

In the long-term ice-sheet run, the appropriate climate at any point in the run is obtained by linearly weighting the surrounding saved climates in the matrix, with the weights proportional to the current austral summer insolation, ice size and logarithm of CO2 level. This matrix-forcing method is discussed further in Pollard (2010). The annual surface mass balance at each point on the ice sheet is calculated from the monthly surface air temperatures and precipitation, using a simple box (zero-dimensional) seasonal surface-mass model that includes snow storage and refreezing of meltwater, and surface melting based on Positive Degree Days (Pollard and DeConto, 2012). The run is initialized with (essentially) no ice. Insolation is based on Laskar et al. (2004). The run is 12 Myr long, nominally from "37 Ma to 25 Ma", although there is little to actually link it to specific paleodates except the Laskar orbits. From 37 to 33 Ma, CO2 decreases linearly from 6xPAL to 2xPAL. From 33 to 25 Ma, CO2 increases linearly from 2xPAL to 10xPAL (where PAL= 280 ppmv). The configuration used to represent MMCO conditions corresponds to 34.8 Ma (CO2 = 3.8xPAL). The one representing MMG conditions, to 33 Ma (CO2=2xPAL).

Lines 82-99 (old numeration; now lines 92-122) have been rewritten.

Section 4: the presentation of the atmospheric pCO2 estimates is rather confused. A distinction between marine and terrestrial proxy-based reconstructions of atmospheric pCO2 has to be done and discussed. Giving only the pCO2 estimates before and after the MMCT transition (corresponding to the two periods studied, MMCO and MMG) rather than the decrease throughout the transition (lines 155-161) would help to clarify the text. I also suggest adding a graph showing the pCO2 estimates in function of time in Ma. This will help to visualize the uncertainties on pCO2 estimates and the suitability of the two concentrations proposed here for MMCO and MMG.

Line 143 (old numeration; now lines 182-187) has been rewritten to indicate which studies provide marine and which terrestrial proxy-based reconstructions, and to discuss the differences in the estimates.

We have removed lines 155-161 (old numeration) and rephrased lines 162-168 (old numeration; now lines 205-214) as follows:

'We chose atmospheric CO_2 concentrations of 400 ppmv and 200 ppmv to represent the MMCO and the MMG respectively (Table 1). Although somewhat arbitrary, these values are within the range of published estimates. The 400 ppmv MMCO is in favourable agreement with Foster et al. (2012) (~392 ppmv at ~15.8 Ma) and Tripati et al. (2009) (~430 ppmv at ~15.1 Ma), although higher than Pearson et al. (2000) (~300 ppmv at ~16.2 Ma) and Pagani et al. (2005) (~300 ppmv at ~15 Ma), and lower than Kürschner et al. (2008) (> ~400-500 ppmv at ~15.5 Ma) and Retallack (2009) (~852 ppmv at ~15.6 Ma) maxima. The 400 ppmv estimate is also in good agreement with the most recent alkenone- and boron isotope-based pCO2

reconstructions for the MMCO by Zhang et al. (2013) and Greenop et al. (2014). The 200 ppmv MMG estimate is in good agreement with Foster et al. (2012) (~200 ppmv at ~12 Ma) and Pagani et al. (2005) (~200 ppmv at ~13 Ma), although higher than Pearson et al. (2000) (~140 ppmv at ~14.7 Ma) and Retallack (2009) (~116 ppmv at ~14.6 Ma), and lower than Tripati et al. (2009) (~340 ppmv at ~12 Ma) and Kürschner et al. (2008) (~280 ppmv at ~14 Ma) minima.'

The reviewer's suggestion of adding a graph showing the pCO2 estimates is interesting, although we do not see the addition of a figure as a requirement for the comprehension of the CO2 section.

Line 163-164: 400 ppmv is not a maximum value of pCO2 for the MMCO if you take into account the reconstructions based on stomatal indices (Kürschner et al., 2008), pedogenic carbonates (Retallack, 2009) and recent estimates based on boron isotopes and alkenones (Foster et al., 2012).

This comment has been taken into account when rephrasing lines 162-168 (old numeration; now lines 205-214) (please, see above).

Subsection 5.3: the description of the gateway reconstruction is too detailed. I suggest putting lines 204 to 214 to the Appendix.

The description at lines 204-214 has been shortened. Nevertheless, it is important that we describe what exact modifications were applied to the dataset of Herold et al. (2008), and the South East Asian gateway is one of the modified areas and an important focus of our study. Hence, we would prefer keeping the whole description as a part of the main text.

Section 6:

Line 249: Herold et al. (2010) prescribed a vegetation distribution derived from Wolfe (1985) using a biome classification for CCSM3 adapted from Bonan et al. (2002). Did you use the same classification here? Could you please discuss the eventual differences between the classifications as they are used with the same land-surface model? I think it could be interesting to add a comparison of your MMCO vegetation reconstruction to the reconstruction proposed in Herold et al. (2010) and to highlight the differences induced by the use of the Pound et al. (2012) dataset.

Unlike Herold et al. (2010), we used the classification described in Bonan et al. (2002) (shown in Table 2 in that study) without modifying it.

Herold et al. (2010) state:

"We classify our vegetation types to a set of biomes modified from Bonan et al. (2002). These modifications include replacing C4 grass with C3 grass, since the former did not become widespread until the late Miocene, and creating a temperate broadleaf evergreen biome to more accurately represent Wolfe's (1985) middle latitude vegetation (c.f. Wolfe, 1985; Bonan et al., 2002)."

Three out of the 28 LSM biomes contain the pft "c4 grass". These biomes are "savanna" (with a 70% of "c4 grass" cover), "warm grassland" (60%), and "cool grassland" (20%) (see Table 2 in Bonan et al., 2002), which do not appear in our reconstruction (Figure 4). Hence, that modification was not required in our representation.

The regions that Herold et. al (2010) painted with the customized LSM biome "temperate broadleaf evergreen forest" (Figure 5 in that study) roughly concide with areas assigned either a) "microphyllous broadleaved evergreen forest", b) "notophyllous broadleaved evergreen forest", c) "mixed broadleaved evergreen and coniferous forest", d) "mixed broadleaved evergreen and deciduous forest", e) "mixed mesophytic forest", or f) "notophyllous woodland/xerophyllous scrub" in the reconstruction from Wolfe (1985).

The "temperate broadleaf evergreen forest" regions in the reconstruction from Herold et. al (2010) appear mostly represented by the BIOME4 biome "warm-temperate evergreen broadleaf and mixed forest" in the reconstruction from Pound et al. (2012). That BIOME4 biome represents either a) "temperate broadleaved evergreen trees" alone, or b) "cool conifer trees" mixed with "temperate broadleaved evergreen trees", or c) "temperate deciduous trees" mixed with either "temperate broadleaved evergreen trees" or "cool conifer trees".

We converted the "warm-temperate evergreen broadleaf and mixed forest" BIOME4 biome into the LSM scheme as "warm mixed forest". The "warm mixed forest" LSM biome contains a mixture of "needleleaf evergreen temperate trees" and "broadleaf deciduous temperate trees".

We agree that the conversion is suboptimal (although the best available), because the pft "broadleaf evergreen temperate tree" is not present in the "warm mixed forest" LSM biome. However, the "warm mixed forest" LSM biome still constitutes a fair representation of the "warm-temperate evergreen broadleaf and mixed forest" BIOME4 biome and the above mentioned vegetation types from Wolfe (1985).

We agree with the reviewer that it would be interesting to compare the reconstruction in Herold et al. (2010) with Figure 4 in our study. Nevertheless, here our scope was to provide a valid reconstruction, by arguing our choice of biomes, and this was accomplished. Therefore, we would like to leave that comparison to the reader.

A note discussing the questions raised by the reviewer has been added at lines 309-320 (new numeration).

Line 263-273: I do not agree with the argument proposed here by the authors. The cooling and drying at mid-latitudes has a non-negligible impact on the vegetation distribution (as also stated by the authors in the Introduction, lines 36-37). This effect could be seen on a 2° x 2° resolution map, or even at the T42-resolution used in the CCSM3 simulations with a more detailed biome classification. This vegetation changes can in turn affect the climate-vegetation interactions (even only via the surface albedo changes) and significantly impact on the global climate. I suggest at least revising the vegetation distribution for the MMG and to detail the biome classification used here in order to better represent the changes between MMCO and MMG vegetation distributions (see General Comment 1).

We agree with the reviewer that the appearance of cooler and drier biomes at mid-latitudes during the Serravallian could have an effect on global climate. Nevertheless, Pound et al. (2012) state that despite these changes the vegetation patterns of the Langhian and Serravallian were "similar" (please, see Figure 5 in Pound et al., 2012), which contrasts with the "markedly different biome pattern of the Tortonian from that of the Serravallian" (please, compare Figure 5 and Figure 6 in Pound et al., 2012).

A clear change in mid-latitude biomes from the Langhian to the Serravallian is visible only in two areas (Figure 5 in Pound et al., 2012): western North America and Europe. During the Serravallian, in the western North American mid-latitudes the "warm-temperate evergreen broadleaf and mixed forest" ("warm mixed forest" in LSM scheme) was still present but other drier/cooler biomes such as "temperate deciduous broadleaf forest" ("warm broadleaf deciduous forest" in LSM scheme) or "cool-temperate mixed forest" ("cool mixed forest" in LSM scheme) had appeared (Pound et al., 2012). In Europe, evidence of cooling/drying during the Serravallian comes from one site in central Spain representing "temperate sclerophyll woodland" ("evergreen shrub land" in LSM scheme), two sites in southern France representing "temperate deciduous broadleaf savanna" ("deciduous shrub land" in LSM scheme), "temperate deciduous broadleaf forest" ("warm broadleaf deciduous forest" in LSM scheme) in southern Germany, and three sites east of 28°E indicating "temperate deciduous broadleaf savanna". Nevertheless, the "warm-temperate evergreen broadleaf and mixed forest" ("warm mixed forest" in LSM scheme) continued to be the main biome in Europe during the Serravallian (Pound et al., 2012).

Thus, for studies with a specific focus on vegetation triggered climatic changes across the MMCT, the user could modify our MMG vegetation dataset (LSM scheme) as follows (based on Pound et al., 2012):

a) In the mid-latitudes of western North America, the "warm mixed forest" between 40-50°N could be partly replaced with "warm broadleaf deciduous forest". Also a "cool mixed forest" could be added in the same region at 42°N.

b) In Europe, some "deciduous shrub land" could be added to the "warm mixed forest" in southern France between 42.5-44°N and 6-9°E, and also between 38-47°N and 29-36°E.

This point is discussed at lines 339-346 (new numeration).

Lines 273-274: how much does the Miocene vegetation distribution differ from the pre-industrial vegetation distribution, as used in CCSM3. It can be useful to briefly list the differences here to better highlight the potential impact of vegetation on the Middle Miocene climate if using the boundary condition set proposed here. I also suggest adding a figure showing the PI vegetation distribution with the same biome classification (maybe in Figure 4).

We have added the following text at lines 350-355 (new numeration):
'Compared to PI, the vegetation of the Middle Miocene represents a warmer and wetter climate. In the northern hemisphere high latitudes forests are warmer, with no forest tundra or tundra present. The mid-latitudes present warmer and wetter biomes, with e.g. less shrub land type biomes. The tropics are wetter, with less savanna and less grasses. There is no evidence for neither a desert in northern Africa (Sahara) nor in central Asia. In the southern hemisphere high latitudes tundra is present at the MMCO and disappears after the Antarctic ice-sheet expansion at the MMG (Pound et al., 2012; Bonan et al., 2002).'

The reader could check Figure 6 in Bonan et al. (2002) for a comparison with modern vegetation in the LSM scheme.

Subsections 6.1 to 6.9: I suggest making these subsections more concise. I would prefer to have only one paragraph focusing on the major vegetation patterns that are taken here into account for the MMCO and MMG. The detailed description of regional vegetation patterns is useless because most of them are neglected for simplification. The authors can directly refer to Pound et al. (2012) for more detailed information.

Although a detailed discussion on the vegetation of each region is not indispensable for the comprehension of this manuscript, we think that it is important to show how exactly we decided what vegetation to assign to each region.

Subsections 6.1-6.9 have thus been moved to the appendix (Section 10; line 622 new numeration), in case the reader was interested in those details.

Section 7:
Lines 467-475: the presentation and discussion of simulation results need to be reworked and extended. What are the global mean surface air temperature and precipitation differences between the two Miocene runs and the PI run? How do you

explain that the MMG run is warmer than the PI run? Is it linked to the absence of ice in the Northern Hemisphere? What is the contribution of the boundary condition changes to the climate differences that the model simulates? A brief comparison with previous modeling studies is highly welcome here. A comparison with some proxy-data (e. g. for SSTs) can also be added.

The global mean surface air temperatures (at 2 m height) are 16.38°C, 13.88°C, and 12.16°C for the MMCO, MMG, and PI experiments, respectively. The global mean precipitation rates are 3.00, 2.86, and 2.72 mm/day for the MMCO, MMG, and PI experiments, respectively.

Potential causes for a MMG climate warmer than PI could be the lower extent of ice-sheets (the Antarctic ice-sheet is smaller and the northern Hemisphere free of ice-sheets in the MMG run), or the different vegetation cover (Knorr et al., 2011). However, unambiguously disentangling the effects of each of the different boundary conditions would require performing a series of sensitivity experiments, which was beyond the scope of the current study. Here our aim was testing the idoneity of the current boundary conditions as input data in GCMs for MMCO and MMG experiments.

Our global mean surface air temperature and precipitation values support the idea of a Middle Miocene climate warmer and wetter than PI, and a cooling and drying trend across the MMCT, as suggested e.g. in Pound et al. (2012).

Mg/Ca data from ODP Hole 1171C on the South Tasman Rise indicate cooling of SST's of ~2°C across the MMCT (Shevenell et. al, 2004). This value is within our range of cooling estimates for the Southern Ocean.

Knorr and Lohmann (2014) MMCT model results show a decrease of 3.1°C in global mean surface air temperature across the MMCT, a value slightly higher than our 2.5°C estimate.

The questions raised by the reviewer have been addressed at lines 570-598 (new numeration).

Concluding remarks: this section needs to be reworked in function of the amendments of the previous sections.

Figures and tables:

Figure 5: I would suggest adding maps of mean surface air temperature differences (MMCO and MMG-PI). It could also be interesting to show the temperature differences between MMCO and MMG.

A map of surface air temperature differences (MMCO-PI and MMG-PI) has been added.

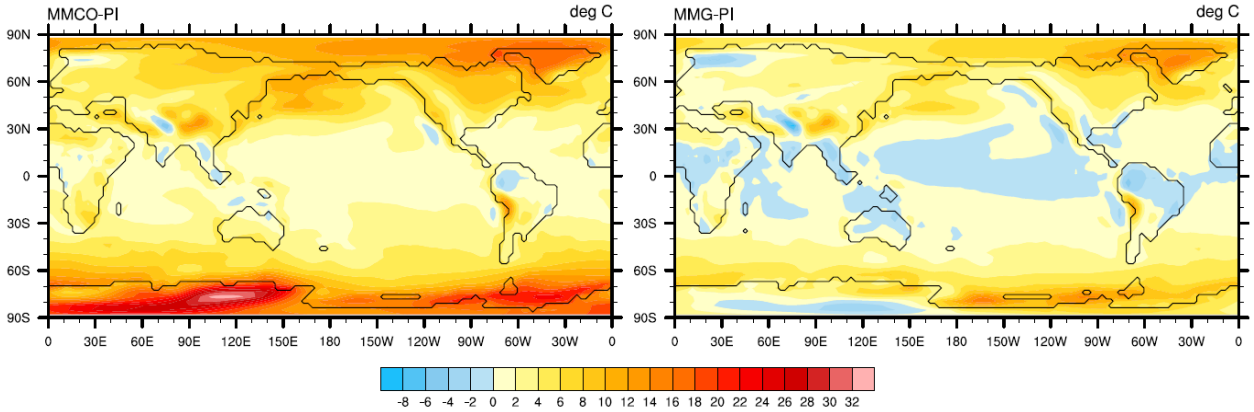

Figure S3: Surface air temperature (at 2 m height) (°C) differences between MMCO and MMG experiments, and PI, respectively.

Table 2: is the correspondence between cool-temperate mixed forest (BIOME 4) and cool mixed forest (LSM) really suitable, since you mention in the footnotes that the cool mixed forest represents only boreal trees? Isn't it another possibility of correspondence?

The "cool-temperate mixed forest" biome represents either a) a forest dominated by "boreal evergreen trees" but with also "temperate deciduous trees" present and a coldest month temperature > -19°C or b) a forest dominated by "temperate deciduous trees" but with also "boreal evergreen trees" present and a coldest month temperature > -15°C.

The "cool mixed forest" biome represents a mixture of "needleleaf evergreen boreal trees" and "broadleaf deciduous boreal trees".

We agree with the reviewer that the correspondence is not optimal, because the deciduous trees in the "cool-temperate mixed forest" are temperate, meanwhile the ones in the "cool mixed forest" are boreal . Nevertheless, there is not a better possibility of correspondence since all the cool forests in the LSM scheme contain only boreal trees (and all the warm forests contain only temperate trees).

Table 3: could you please give explicitly the values of the model parameters instead of citing a reference paper? Same for the PI orbital parameters.

Done. Please, see the updated table below.

Experiment	PI	MMCO	MMG
CO_2	280 ppmv	400 ppmv	200 ppmv
CH_4	760 ppbv	same as PI	
N_2O	270 ppbv		
CFC's	0		
O_3	1870 A.D.		
Sulfate aerosols	1870 A.D.		
Dust and sea salt	PD		
Carbonaceous aerosols	30% of PD		
Solar constant	1365 Wm^{-2}		
Eccentricity	0.016724		
Obliquity	23.446 °		
Precession	102.04 °		

Table 3: Summary of atmospheric composition, solar constant, and orbital configuration for the CCSM3 test experiments. PI values are according to Otto-Bliesner et al. (2006). The orbital configuration represents 1950 A.D. values. PD = present day.

Further details on the ozone and sulfate aerosols distribution can be found in Otto-Bliesner et al. (2006).

Technical comments:

-Line 50: replace “passages” by “seaways”

Replaced.

-Line 51: add the precision “most previous Middle Miocene studies with prescribed vegetation”

Added.

-Lines 56-57: could you please rephrase this sentence? There are other ways to produce boundary condition assemblages.

Done.
Rephrased as:
'Despite the relatively low availability of Middle Miocene data'.

-Line 93: replace “6 estimate” by “volume estimate”

Replaced (now line 95).

-Line 133: write “previous Section”

The journal guidelines under https://www.geoscientific-model-development.net/for_authors/manuscript_preparation.html suggest writing Sect. instead of Section, unless that word appears at the beginning of a sentence.
The instructions state literally:
'The abbreviation "Sect." should be used when it appears in running text and should be followed by a number unless it comes at the beginning of a sentence.'

-Line 165: delete the space between “p” and “CO2”

Done.

-Line 178: “ice-free conditions”

Done. "ice free" has been replaced with "ice-free", at line 178 and, for consistency, in all other occcurrences in the text.

-Line 191: replace “passages” by “seaways”

Done.

-Line 194: write “Section 2”:

Please, see above our answer to the comment to Line 133.

-Line 230: could you please use “seaway” instead of passage or Central American seaway.

Done.
"Panama passage" has been replaced with "Panama seaway". Also at Line 231 (old numeration).

-Line 312: “Northeast Australia”

The following is stated in the journal guidelines under
https://www.geoscientific-model-development.net/for_authors/manuscript_preparation.html:

'Cardinal directions should only be capitalized when part of a proper noun (e.g. South Dakota, Northern Ireland, North America, but eastern France).'

-Lines 318, 320: “East Australia”

Please, see above.

-Line 322 and after: I always put a caption letter to subregions or continents “West Australia”, “Southern Africa”, etc.

Please, see above.

-Line 448: please explain configuration T42x1 or detail.

T42 is the atmosphere horizontal grid, a Gaussian grid with 64 points in latitude and 128 points in longitude (~2.8° resolution). The notation T42 refers to the spectral truncation level. x1 is the ocean horizontal grid, a dipole grid with 384 points in latitude and 320 points in longitude. The zonal resolution of the ocean horizontal grid is ~1°, the mean meridional resolution is ~0.5°, refined around the equator (~0.3°). The notation x1 refers to the nominal zonal resolution. T42x1 is the model configuration employing the T42 and x1 grids.

Lines 448-453 (old numeration) have been modified as follows:

'The atmosphere horizontal grid employed in the PI run, T42, is a Gaussian grid with 64 points in latitude and 128 points in longitude (~2.8° resolution). The notation T42 refers to the spectral truncation level. The land and atmosphere models share the same horizontal grid. The ocean horizontal grid, x1, is a dipole grid with 384 points in latitude and 320 points in longitude. The zonal resolution of the ocean horizontal grid is ~1°, the mean meridional resolution is ~0.5°, refined around the equator (~0.3°). The notation x1 refers to the nominal zonal resolution. The ocean and sea–ice components share the same horizontal grid. The atmosphere and ocean vertical grids have 26 and 40 vertical levels, respectively. This model grid configuration is known as T42x1.'

-Line 464: “archived as b30.043” does this information really need to be mentioned?

It is not indispensable. We removed it.

Additional modifications:

-Line 51 (now line 59): "were mainly based" was gramatically incorrect. It was replaced with "was mainly based".

-Line 237 (now line 295): 15.67 has been replaced with 15.97. The Langhian expands the interval 15.97– 13.65 Ma

-Lines 460-463 (now lines 559-560): The orbital configuration used in the Miocene experiments is identical to the one used in the PI experiment. There was a mistake in our statement there, sorry about that. Those lines were rephased as follows to correct the mistake:

'Well-mixed greenhouse gases, ozone, aerosols, solar constant and orbital configuration were kept the same as in PI, except for CO2 (Table 3).'

-Line 493 (now line 618): we replaced "2°x2° lat/lon grid" with "0.5°x0.5° lat/lon grid". Although Herold et al. (2008) topography/bathymetry dataset was provided to us in a 2°x2° resolution, we regridded it to a finer resolution (0.5°x0.5°) for our purposes.

-Lines 492-495 (now lines 616-621): a reference to the CCSM3 model output files from the MMCO, MMG, and PI experiments included in the supplement has been added.

We hope we have addressed all your comments.

Yours sincerely,

Amanda Frigola and co-authors.

References:

Alder, J. R., Hostetler, S. W., Pollard, D., and Schmittner, A.: Evaluation of a present-day climate simulation with a new coupled atmosphere-ocean model GENMOM, GMD, 4(1), 69–83, doi:10.5194/gmd-4-69-2011, 2011.

Bonan, G. B., Levis, S., Kergoat, L., and Oleson, K.W.: Landscapes as patches of plant functional types: An integrating concept for climate and ecosystem models, Global Biogeochemical Cycles, 16(2), 5-1–5-23, doi:10.1029/2000GB001360, 2002.

Foster, G. L., Lear, C. H., and Rae, J. W. B.: The evolution of pCO2, ice volume and climate during the middle Miocene, Earth Planet. Sc. Lett., 341–344, 243–254, doi:10.1016/j.epsl.2012.06.007, 2012.

Gasson, E., DeConto, R. M., Pollard, D. and Levy, R. H.: Dynamic Antarctic ice sheet during the early to mid-Miocene, P. Natl. Acad. Sci., 113(13), 3459–3464, doi:10.1073/pnas.1516130113, 2016.

Greenop, R., Foster, G. L., Wilson, P. A. and Lear, C. H.: Middle Miocene climate instability associated with high-amplitude CO2 variability, Paleoceanography, 29(9), 845–853, doi:10.1002/2014PA002653, 2014.

Henrot, A.-J., Utescher, T., Erdei, B., Dury, M., Hamon, N., Ramstein, G., Krapp, M., Herold, N., Goldner, A., Favre, E., Munhoven, G., and François, L.: Middle Miocene climate and vegetation models and their validation with proxy data, Palaeogeogr. Palaeoclimatol. Palaeoecol., 467, 95–119, doi:10.1016/j.palaeo.2016.05.026, 2017.

Herold, N., Seton, M., Müller, R. D., You, Y. and Huber, M.: Middle Miocene tectonic boundary conditions for use in climate models, Geochem. Geophy. Geosy., 9(10), Q10009, doi:10.1029/2008GC002046, 2008.

Herold, N., Müller, R., and Seton, M.: Comparing early to middle Miocene terrestrial climate simulations with geological data, Geosphere, 6 (6), 952–961, doi:10.1130/GES00544.1, 2010.

Knorr, G., Butzin, M., Micheels, A., Lohmann, G.: A warm Miocene climate at low atmospheric CO_2 levels, Geophysical Research Letters, 38(20), L20701, doi:10.1029/2011GL048873, 2011.

Knorr, G. and Lohmann, G.: Climate warming during Antarctic ice sheet expansion at the Middle Miocene transition, Nature Geoscience, 7(5), 376–381, doi:10.1038/ngeo2119, 2014.

Kuerschner, W. M., Kvacek, Z. and Dilcher, D. L.: The impact of Miocene atmospheric carbon dioxide fluctuations on climate and the evolution of terrestrial ecosystems, P. Natl. Acad. Sci., 105(2), 449–453, doi:10.1073/pnas.0708588105, 2008.

Laskar, J., Robutel, P., Joutel, F., Gastineau, M., Correia, A. C. M., Levrard, B.: A long term numerical solution for the insolation quantities of the Earth, 428, 261-285, A&A, doi:10.1051/0004-6361:20041335, 2004.

Le Brocq, A. M., Payne, A. J., and Vieli, A.: An improved Antarctic dataset for high resolution numerical ice sheet models (ALBMAP v1), Earth Syst. Sci. Data., 2 (2), 247-260, doi:10.5194/essd-2-247-2010, 2010.

Morley, R. J.: Cretaceous and Tertiary climate change and the past distribution of megathermal rainforests, in: Tropical Rainforest Responses to Climatic Change, Bush, M., Flenley, J., Gosling, W., Springer Praxis Books, Berlin, Heidelberg, 1-34, 2011.

Otto-Bliesner, B. L., Tomas, R., Brady, E. C., Ammann, C., Kothavala, Z., and Clauzet, G.: Climate sensitivity of moderate and low resolution versions of CCSM3 to preindustrial forcings, J. Climate, 19, 2567–2583, doi:10.1175/JCLI3754.1, 2006.

Pagani, M., Zachos, J. C., Freeman, K. H., Tipple, B., Bohaty, S.: Marked Decline in Atmospheric Carbon Dioxide Concentrations During the Paleogene, Science, 309(5734), 600–603, doi:10.1126/science.1110063, 2005.

Pearson, P. N. and Palmer, M. R.: Atmospheric carbon dioxide concentrations over the past 60 million years, Nature, 406(6797), 695–699, doi:10.1038/35021000, 2000.

Pollard, D.: A retrospective look at coupled ice sheet–climate modeling, Clim. Change, 100, 173-194, doi:10.1007/s10584-010-9830-9, 2010.

Pollard, D. and DeConto, R. M.: Description of a hybrid ice sheet-shelf model, and application to Antarctica, Geosci. Model Dev., 5, 1273-1295, doi:10.5194/gmd-5-1273-2012, 2012.

Pound, M. J., Haywood, A. M., Salzmann, U. and Riding, J. B.: Global vegetation dynamics and latitudinal temperature gradients during the Mid to Late Miocene (15.97–5.33Ma), Earth- Sci. Rev., 112(1–2), 1–22, doi:10.1016/j.earscirev.2012.02.005, 2012.

Retallack, G. J.: Refining a pedogenic-carbonate CO2 paleobarometer to quantify a middle Miocene greenhouse spike, Palaeogeogr. Palaeocl., 281(1–2), 57–65, doi:10.1016/j.palaeo.2009.07.011, 2009.

Shevenell, A. E., Kennett, J. P., Lea, D.W.: Middle Miocene Southern Ocean Cooling and Antarctic Cryosphere Expansion, Science, 305(5691), 1766-1770, doi:10.1126/science.1100061, 2004.

Tripati, A. K., Roberts, C. D. and Eagle, R. A.: Coupling of CO2 and Ice Sheet Stability Over Major Climate Transitions of the Last 20 Million Years, Science, 326(5958), 1394–1397, doi:10.1126/science.1178296, 2009

Wolfe, J.A.: Distribution of major vegetational types during the Tertiary, in: The carbon cycle and atmospheric CO2: natural variations Archean to present, edited by: Sundquist E. T. and Broecker W. S., American Geophysical Union Monograph, 32, 357–375, doi:10.1029/GM032p0357, 1985.

Zhang, Y. G., Pagani, M., Liu, Z., Bohaty, S. M., and DeConto, R.: A 40-million-year history of atmospheric CO2, Philos. Trans. R. Soc. A, 371(2001), 20130096, doi:10.1098/rsta.2013.0096, 2013.

Boundary conditions for the Middle Miocene Climate Transition (MMCT v1.0)

Amanda Frigola[1], Matthias Prange[1,2], Michael Schulz[1,2]

[1]MARUM Center for Marine Environmental Sciences, University of Bremen, Bremen, 28359, Germany

[2]Faculty of Geosciences, University of Bremen, Bremen, 28359, Germany

Correspondence to: Amanda Frigola (afrigola@marum.de)

Abstract. The Middle Miocene Climate Transition was characterized by major Antarctic ice-sheet expansion and global cooling during the interval ~15–13 Ma. Here we present two sets of boundary conditions for global general circulation models characterizing the periods before (Middle Miocene Climatic Optimum; MMCO) and after (Middle Miocene Glaciation; MMG) the transition. These boundary conditions include Middle Miocene global topography, bathymetry and vegetation. Additionally, Antarctic ice volume and geometry, sea-level and atmospheric CO_2 concentration estimates for the MMCO and the MMG are reviewed. The MMCO and MMG boundary conditions have been successfully applied to the Community Climate System Model version 3 (CCSM3) to provide evidence of their suitability for global climate modeling. The boundary-condition files are available for use as input in a wide variety of global climate models and constitute a valuable tool for modeling studies with a focus on the Middle Miocene.

1 Introduction

The Middle Miocene (ca. 16–11.6 Ma) was marked by important changes in global climate. The first stage of this time period, the Middle Miocene Climatic Optimum (MMCO), was characterized by warm conditions, comparable to those of the late Oligocene. Although global climate remained warmer than present-day during the whole Miocene (Pound et al., 2012), an important climate transition associated with major Antarctic ice-sheet expansion and global cooling took place between ~15 and 13 Ma, the so called Middle Miocene Climate Transition (MMCT). ~~Our work has its focus on the Middle Miocene Climate Transition (MMCT), an interval of climate change characterized by significant Antarctic ice-sheet expansion and global cooling between ~15 and 13 Ma.~~ Major evidence for this transition is the increase in $\delta^{18}O$ shown in benthic foraminiferal records (e.g. Lear et al., 2010; Shevenell et al., 2008; Holbourn et al., 2005).

An increase in benthic foraminiferal $\delta^{18}O$ reflects either an increase in global ice volume, ~~or~~ a decrease in bottom water temperature (BWT), or a combination of both. Different studies using benthic foraminiferal Mg/Ca ratios (an independent proxy for BWT) to separate the global ice volume from BWT signals in the benthic foraminiferal $\delta^{18}O$ records conclude that

both an increase in global ice volume and a decrease in BWT occurred during the MMCT, though global ice volume was the main part (65–85%) in the benthic $\delta^{18}O$ signal (Lear et al., 2010; Lear et al., 2000; Shevenell et al., 2008).

Mg/Ca studies indicate that the cooling of bottom waters across the MMCT was~~would have been~~ within a range of ~0.5 to ~3°C (Lear et al., 2010; Lear et al., 2000; Shevenell et al., 2008; Billups and Schrag, 2002; Billups and Schrag, 2003).

Studies by Kominz et al. (2008) and Haq et al. (1987), based on backstripping techniques, and John et al. (2011), combining backstripping techniques with benthic foraminiferal $\delta^{18}O$, indicate an important eustatic sea-level fall across the MMCT (see Sect. 3), providing further evidence of ice-sheet expansion. Lewis et al. (2007) present data from glacial deposits in Southern Victoria Land (East Antarctica) showing local ice-sheet expansion at different time intervals between ~13.85 and ~12.44 Ma. They state that this ice-sheet expansion was preceded by significant atmospheric cooling, with glacial deposits showing evidence of a permanent shift from wet to cold in the thermal regime of local glaciers at ~13.94 Ma. Levy et al. (2016) analyze data from the ANDRILL–2A drill site, situated in the western Ross Sea, ~30 km off the coast of Southern Victoria Land. The ANDRILL record presents two unconformities spanning the intervals ~15.8 to ~14.6 Ma and ~14.4 Ma to Late Miocene. These unconformites are interpreted to be caused by local episodes of grounded ice advance eroding material at the site at different times within those two intervals. A global compilation of paleobotanical data by Pound et al. (2012) shows cooling and/or drying in some mid-latitude areas across the MMCT, suggesting that this transition did not only affect high latitudes.

The causes for the MMCT are a matter of debate. Suggested driving mechanisms for this transition include a drop in atmospheric pCO_2, changes in ocean circulation and water masses driven by ocean gateways reconfiguration and/or orbitally triggered atmospheric heat and moisture transport variations (Flower and Kennett, 1994; Holbourn et al., 2007; Holbourn et al., 2005). Langebroek et al. (2010), for example, using an isotope enabled ice-sheet–climate model forced with a pCO_2 decrease and varying time-dependent orbital parameters, modeled an increase in $\delta^{18}O$ of sea water in good agreement with published MMCT estimates.

Our aim is to assemble Middle Miocene boundary conditions for global coupled General Circulation Models (GCMs), setting up an improved basis to investigate the MMCT from a modeling perspective. The boundary conditions include global topography, bathymetry and vegetation for the Middle Miocene (see Sect. 9). Besides, Antarctic ice volume and geometry, sea-level and atmospheric CO_2 concentration estimates for the periods before (Middle Miocene Climatic Optimum, MMCO) and after (Middle Miocene Glaciation, MMG) the MMCT are reviewed and their uncertainties are discussed. The global topography and bathymetry presented here are mainly based on the Middle Miocene reconstruction by Herold et al. (2008), which has already been used in previous modeling studies (e.g. Herold et al., 2012; Herold et al., 2011; Krapp and Jungclaus, 2011). However, we implement some important modifications with regard to Antarctic ice-sheet geometry, sea-level and configuration of the South East Asian and Panama seaways~~passages~~ taking into account recent reconstructions. Vegetation cover used in most previous Middle Miocene modeling studies with prescribed vegetation was~~were~~ mainly based on Wolfe's

(1985) Early Miocene reconstruction (e.g. Herold et al., 2011; Tong et al., 2009; You et al., 2009). Here, also Middle Miocene data (Pound et al., 2012; Morley, 2011) have been used ~~we update these boundary conditions with Middle Miocene data (Pound et al., 2012; Morley, 2011)~~.

Our study provides the core boundary conditions~~data~~ required to set up GCM experiments with a Middle Miocene configuration. With this configuration as a starting point, a wide variety of sensitivity studies with a focus on the Middle Miocene and its global climate transition can be performed. Despite the relatively low availability of Middle Miocene data~~scarce Middle Miocene data availability and method related uncertainties in the data~~, our assemblage of boundary conditions reflects the state-of-the-art in Miocene research. Results from two model runs with the Community Climate System Model version 3 (CCSM3) (Collins et al., 2006) using the MMCO and MMG boundary conditions are also presented.

2 Antarctic ice-sheet geometry

Giving quantitative Antarctic ice volume estimates for the MMCT is at best challenging. Most sediment core studies present ice volume estimates in units of sea water $\delta^{18}O$. Backstripping methods provide sea-level rather than ice volume estimates. More direct Antarctic ice volume estimates can be derived from modelling studies (Gasson et al., 2016; Langebroek et al., 2009; Oerlemans 2004).

Gasson et al. (2016) performed a series of simulations with an ice-sheet model asynchronously coupled to a regional climate model and an isotope-enabled GCM using Middle Miocene palaeogeography and a range of atmospheric CO_2 concentrations and extreme astronomical configurations. The study~~simulations~~ tested two different Antarctic bedrock topography scenarios: one scenario with present day bedrock topography and the other one with an approximate Middle Miocene bedrock topography. For a range of CO_2 concentrations between 500 and 280 ppmv and changing orbital parameters ("warm astronomical configuration" versus "cold astronomical configuration") an increase in Antarctic ice volume from 11.5 (17.2) million km³ in the warmer climate to 26.7 (35.5) million km³ in the colder climate was simulated using modern (Middle Miocene) bedrock topography.

Langebroek et al. (2009) used a coupled ~~isotope-enabled~~ ice-sheet–climate model forced by atmospheric CO_2 and insolation changes to reconstruct Antarctic ice volume across the MMCT. The experiment with the best fit to $\delta^{18}O$ data was forced by a CO_2 drop from 640 ppmv to 590 ppmv at around ~13.9 Ma and simulates an increase in Antarctic ice volume from ~6 million to ~24 million km³ across the MMCT.

Oerlemans (2004) derived Cenozoic Antarctic ice volume variations by means of a simple quasi-analytical ice-sheet model and two different $\delta^{18}O$ benthic foraminiferal records. The ice-sheet model approximates Antarctic ice volume as a function of deep sea temperature. Using the Zachos et al. (2001) benthic foraminiferal $\delta^{18}O$ data, an ice volume increase from ~5 million

to ~23 million km³ for the MMCT was obtained, while for the $\delta^{18}O$ curve by Miller et al. (1987) the increase was only from ~15 million to ~23 million km³.

Mainly based on the studies by Oerlemans (2004) and Langebroek et al. (2009), we set a total Antarctic ice-sheet volume of 23 million km³ for the MMG (Table 1; Fig. 1). This value is within the range of published estimates, although smaller than the values estimated by Gasson et al. (2016) in their "cold climate" experiments with extreme astronomical configuration. For the MMCO we assume a total Antarctic ice-sheet volume of 6 million km³. This volume estimate is in good agreement with the values given by Langebroek et al. (2009) and Oerlemans (2004), although significantly lower than Gasson et al. (2016) (see above).

In this study, ~~W~~we opted for using ice-sheet model-derived Antarctic topography estimates from an earlier Cenozoic time period with similar Antarctic ice volume. These data were kindly provided by David Pollard (Pennsylvania State University) and correspond to the Oligocene Oi-1 glaciation event~~, approximately 34 Ma~~. They were obtained with a model version close to that described in Pollard and DeConto (2012), but with no marine ice physics, so that any floating ice is immediately removed. The bedrock-elevation boundary conditions used in that run are from the modern ALBMAPv1 dataset (Le Brocq et al., 2010). Climate forcing is obtained from a matrix of GCM climates for various orbits, CO_2 levels and ice sizes (Pollard, 2010). Insolation is based on Laskar et al. (2004). The run is 12 Myr long, nominally from "37 Ma to 25 Ma". The configuration we used to represent MMCO conditions corresponds to 34.8 Ma; the one representing MMG conditions, to 33 Ma.~~ with the main differences being (i) no floating ice shelves, and (ii) climate forcing using a matrix of previous GCM climates for various orbits, CO_2 levels and ice sizes. These topography data provide a fair characterization of the Antarctic ice-sheet at the MMG as they match a total ice volume of 23 million km³.~~

In the~~this~~ MMG configuration~~topography~~ the whole East Antarctica is covered with a single ice-sheet meanwhile the islands of West Antarctica contain only some small ice caps, with no marine-based ice-sheets ~~(Fig. 1)~~. In the MMCO configuration Antarctica is only partially glaciated, with an ice cap covering the Transantarctic Mountains and another one over eastern East Antarctica. Again, West Antarctica contains only some ice caps, with no marine-based ice-sheets (Fig. 1). We deem the ice configurations from the Oi-1 glaciation run appropriate for the MMCT as they match total ice volumes of 23 million km³ for the MMG and of 6 million km³ for the MMCO, values that are within the range of published ice volume estimates for the MMG and MMCO, respectively. Besides, there is little to link Pollard's run to a specific time period (except for the Laskar orbits). The configurations of Oerlemans (2004) and Langebroek et al. (2009) were discarded in our study because they are rather simple (no two-dimensional representation of the Antarctic ice-sheet is available from those studies). The configuration of Gasson et al. (2016) could be considered in future sensitivity studies, since uncertainties in ice volume estimates are high. Nevertheless, the distribution of ice in our study is comparable to that in Gasson et al. (2016): for the MMG, a continental-scale ice-sheet exists in East Antarctica with ice thicknesses of ~3000-4000 m, although in West

Antarctica there is less ice in Pollard's data; for the MMCO, the ice-sheets occupy similar positions, although they are less extensive in Pollard's data.

~~For the MMCO we assume a total Antarctic ice-sheet volume of 6 million km³ (Table 1, Fig. 1). This 6 estimate is in good agreement with the values given by Langebroek et al. (2009) and Oerlemans (2004), although significantly lower than Gasson et al. (2016) (see above).~~

~~To characterize the MMCO Antarctic topography, again David Pollard's data from the same Oi-1 simulation were used, which match an Antarctic ice volume of 6 million km³. In this topography Antarctica is only partially glaciated, with an ice cap covering the Transantarctic Mountains and another one over eastern East Antarctica. Again, West Antarctica contains only some ice caps, with no marine based ice-sheets (Fig. 1).~~

The ice volume values of 6 million and 23 million km³ for the MMCO and the MMG, respectively, imply an increase of 17 million km³ across the MMCT. This value is within the range of published estimates and in reasonable agreement with the values by Langebroek et al. (2009), Oerlemans (2004) as well as Gasson et al. (2016) (see above).

Although some studies suggest ice would have been present in the Northern Hemisphere during the Middle Miocene (Thiede et al., 2011; DeConto et al., 2008), little~~very few~~ is known about its temporal and spatial distribution. In view of the lack of concrete data, Northern Hemisphere ice was neglected in the current study.

3 Sea-level change across the MMCT

For the sake of coherency within the current set of Middle Miocene boundary conditions, we opted for a sea-level change across the MMCT that is consistent with our ice-sheet volume estimates for the MMCO and MMG (see previous Sect.), presuming that global sea-level change across the MMCT time interval was dominated by glacio-eustasy. The ice-sheet volume estimates were converted into sea-level equivalents according to the following equation (Langebroek et al., 2009):

$$S_{eq} = (\rho_{ice} * V_{ice}) / (\rho_{water} * A_0) \quad (1)$$

where S_{eq} represents sea-level equivalent, V_{ice} ice-sheet volume, ρ_{ice} density of ice, ρ_{water} density of water and A_0 ocean surface area. With $\rho_{ice} = 910$ kg/m³, $\rho_{water} = 1000$ kg/m³ and $A_0 = 360.5$ million km² (present-day approx.), values of 16 and 59 m for the MMCO and the MMG respectively were obtained (as in Langebroek et al., 2009), and thus a sea-level fall across the MMCT of 43 m (Table 1).

Lear et al. (2010) combine Mg/Ca and Li/Ca ratios to estimate BWT at ODP Site 761 across the MMCT. Sea water $\delta^{18}O$ is then derived by extracting the BWT signal from the $\delta^{18}O$ signal from the same site. The data suggest an increase in sea water $\delta^{18}O$ of 0.6 per mil between 15.3 and 12.5 Ma. This value is converted into a sea-level fall equivalent using the Pleistocene calibration of 0.08–0.11 per mil per 10 m sea-level (Fairbanks and Matthews, 1978), obtaining an eustatic sea-level drop of ~55–75 m between 15.3 and 12.5 Ma.

~~Langebroek et al. (2009) suggested Antarctic ice volumes of ~6 million and ~24 million km³ for the MMCO and the MMG, respectively (see previous Sect.). These ice volume estimates can be converted into sea-level equivalents according to:~~

~~$S_{eq} = (\rho_{ice} * V_{ice}) / (\rho_{water} * A_0)$ (1)~~

~~where S_{eq} represents sea-level equivalent, V_{ice} ice-sheet volume, ρ_{ice} density of ice, ρ_{water} density of water and A_0 ocean surface area. With ρ_{ice} = 910 kg/m³, ρ_{water} = 1000 kg/m³ and A_0 = 360.5 million km² (present-day approx.), the resulting sea-level equivalents are ~16 and ~59 m for the MMCO and MMG, respectively, implying a sea-level fall of ~43 m across the MMCT.~~

De Boer et al. (2010) used one-dimensional ice-sheet models and benthic foraminiferal $\delta^{18}O$ data (Zachos et al., 2008) to derive eustatic sea-level and BWT changes over the last 35 Ma. In their approach, surface air temperature has been derived through an inverse procedure from the benthic $\delta^{18}O$ record. The study suggests a sea-level drop of ~40 m between 15 and 12 Ma, i.e., from ~55 to ~15 m above present-day.

Kominz et al. (2008) combine data from different boreholes collected from the New Jersey and Delaware Coastal Plains to derive sea-level for the last 108 Ma through backstripping. They register a ~20 m sea-level fall between ~14.2 and ~12.8 Ma, i.e., from ~25 to ~5 m above present day. These data contain some unconformities however, implying that the actual amplitude of the MMCT sea-level drop could have been indeed higher than proposed there.

John et al. (2011) estimate Middle Miocene sea-level changes based on backstripping and benthic foraminiferal oxygen isotope data. Backstripping is applied to sediment core data from the Marion Plateau, offshore Northeastern Australia, obtaining a range of sea-level variations which is then further constrained using benthic foraminiferal $\delta^{18}O$ data from Zachos et al. (2001). John et al. (2011) suggest a 53–69 m sea-level fall between 16.5 and 13.9 Ma. Unfortunately, their analyses are limited to this time interval.

~~For the sake of coherency within the current set of Middle Miocene boundary conditions, we opted for a sea-level change across the MMCT that is consistent with our ice-sheet volume estimates for the MMCO and MMG (see previous Sect.), presuming that global sea-level change across the MMCT time interval was dominated by glacio-eustasy. The ice-sheet volume estimates were converted into sea-level equivalents according to Eq. (1), obtaining values of 16 and 59 m for the MMCO and the MMG respectively, and thus a sea-level fall across the MMCT of 43 m (Table 1).~~

Our~~A~~ sea-level fall estimate of 43 m across the MMCT is consistent with Langebroek et al. (2009~~10~~) (~43 m) and in good agreement with the study by De Boer et al. (2010) (~40 m), although somewhat larger than the values by Gasson et al. (2016) (~30–36 m) and considerably higher than Kominz et al. (2008) estimate (~20 m of sea-level fall). By contrast, John et al. (2011) suggest a higher amplitude of sea-level drop (~53–69 m), similar to the ~55–75 m by Lear et al. (2010). As such, our assumption of 43 m sea-level fall lies well within the range of published estimates.

4 Atmospheric CO_2 concentration

Numerous studies based on both marine (Foster et al., 2012; Pearson and Palmer, 2000; Tripati et al., 2009; Pagani et al., 2005) and terrestrial (Retallack, 2009; Kuerschner et al., 2008) proxies reconstructing Middle Miocene atmospheric CO_2 levels are present in the literature. However, the range of published estimates is rather wide. ~~Middle Miocene atmospheric pCO_2 is a matter of debate as different studies suggest significantly different pCO_2 levels.~~ The difference in the CO_2 estimates between the various studies arises most likely from method-related uncertainties and/or the relatively coarse temporal resolution of some of the datasets. Based on planktonic foraminiferal boron isotopic data, Foster et al. (2012) suggest atmospheric pCO_2 values reaching a maximum of ~390 ppmv at ~15.8 Ma and decreasing to ~200 ppmv by ~12 Ma. Pearson and Palmer (2000), using the same method, obtain a maximum value of ~300 ppmv at ~16.2 Ma followed by a decline to ~140 ppmv by ~14.7 Ma and an increase to ~225 ppmv by ~11.4 Ma. Tripati et al. (2009), by means of surface-dwelling foraminiferal boron/calcium ratios, obtain a maximum value of ~430 ppmv at ~15.1 Ma followed by a decrease to ~340 ppmv by ~12 Ma and down to ~230 ppmv by ~9.9 Ma. Retallack (2009), based on carbon isotopes of pedogenic carbonate, suggests atmospheric pCO_2 levels reaching a maximum of ~850 ppmv at ~15.6 Ma, dropping down to ~115 ppmv by ~14.6 Ma and increasing to ~430 ppmv by ~12.8 Ma. Kuerschner et al. (2008) used stomatal-density data from fossil leaves to support pCO_2 values reaching a maximum over ~400–500 ppmv at ~15.5 Ma, decreasing to ~280 ppmv by ~14 Ma and increasing to ~340 ppmv by ~12 Ma. By contrast, Pagani et al. (2005), using a method based on alkenone carbon isotopes, obtain pCO_2 values oscillating between ~200 ppmv and ~300 ppmv across the Middle Miocene.

~~In spite of the tremendous discrepancies between studies, all except for Pagani et al. (2005) agree on an atmospheric pCO_2 drawdown starting at the MMCO. The exact magnitude of this decrease is however not clear: ~190 ppmv between ~15.8 and ~12 Ma according to Foster et al. (2012), ~160 ppmv between ~16.2 and ~14.7 Ma or ~75 ppmv between ~16.2 and ~11.5 Ma according to Pearson and Palmer (2000), ~90 ppmv between ~15.1 and ~12 Ma or ~200 ppmv between ~15.1 and ~9.9 Ma according to Tripati et al. (2009), ~740 ppmv between ~15.6 and ~14.6 Ma or ~420 ppmv between ~15.6 and ~12.8 Ma according to Retallack (2009), and over ~120–220 ppmv between ~15.5 and ~14 Ma or over ~60–160 ppmv between ~15.5 and ~12 Ma according to Kuerschner et al. (2008).~~

We chose atmospheric CO_2 concentrations of 400 ppmv and 200 ppmv to represent the MMCO and the MMG respectively (Table 1). Although somewhat arbitrary, these values are within the range of published estimates. The 400 ppmv MMCO is in favourable agreement with Foster et al. (2012) (~392 ppmv at ~15.8 Ma) and Tripati et al. (2009) (~430 ppmv at ~15.1 Ma), although higher than Pearson et al. (2000) (~300 ppmv at ~16.2 Ma) and Pagani et al. (2005) (~300 ppmv at ~15 Ma), and lower than Kürschner et al. (2008) (> ~400-500 ppmv at ~15.5 Ma) and Retallack (2009) (~852 ppmv at ~15.6 Ma) maxima. The 400 ppmv estimate is also in good agreement with the most recent alkenone- and boron isotope-based pCO2 reconstructions for the MMCO by Zhang et al. (2013) and Greenop et al. (2014). The 200 ppmv MMG estimate is in good agreement with Foster et al. (2012) (~200 ppmv at ~12 Ma) and Pagani et al. (2005) (~200 ppmv at ~13 Ma), although

higher than Pearson et al. (2000) (~140 ppmv at ~14.7 Ma) and Retallack (2009) (~116 ppmv at ~14.6 Ma), and lower than Tripati et al. (2009) (~340 ppmv at ~12 Ma) and Kürschner et al. (2008) (~280 ppmv at ~14 Ma) minima.' ~~The 400 ppmv MMCO estimate represents a maximum rather than a mean (within the interval ~15–17 Ma) and is in favourable agreement with Foster et al. (2012) and Tripati et al. (2009), as well as with the most recent alkenone- and boron isotope-based pCO_2 reconstructions for the MMCO by Zhang et al. (2013) and Greenop et al. (2014). The 200 ppmv MMG estimate represents a minimum rather than a mean (within the interval ~12–15 Ma) and is in good agreement with Foster et al. (2012) and Pagani et al. (2005).~~

5 Global topography and bathymetry

We present here two different global Middle Miocene topography/bathymetries, characterizing the MMCO and the MMG periods (Fig. 2, Table 1, Sect. 9). Both global topography/bathymetries are mainly based on the 2°x2° reconstruction of Herold et al. (2008), although some important modifications, which will be described below, were applied to their original dataset. To reconstruct paleogeography and paleotopography Herold et al. (2008) used a global plate rotation model and geological data. Ocean depth was reconstructed by applying an age–depth relationship to a global Middle Miocene isochron map. Sediment thickness and large igneous provinces were also considered in the reconstruction of ocean depth.

In Herold et al. (2008), the Andes and the Tibetan plateau were set with estimated Early to Middle Miocene elevations. The Rocky M~~m~~ountains and the east African topography were reduced to 75 and 25% of their current elevation, respectively. The Greenland topography was also reduced, representing ice-~~-~~free conditions. The Bering Strait was closed and the Hudson Bay removed. Unlike Herold et al. (2008), who assumed the Tethys seaway closed, we decided to leave the seaway open. According to Rögl (1999), the Tethys passage closed during the Burdigalian (20.44–15.97 Ma), re-opened temporary during the Langhian (15.97–13.65 Ma) and closed again during the Serravallian (13.65–11.62 Ma). Also based on Rögl (1999), the Paratethys was intermittently connected and disconnected from the global ocean during the Burdigalian to Serravallian interval. In Herold et al. (2008), as in our reconstruction, the Paratethys is connected to the global ocean. In view of the variable configuration of the Tethys/Paratethys across the Middle Miocene, it would be recommendable to test different Tethys/Paratethys configurations when performing Middle Miocene experiments with GCMs, although such testing can be limited by model constraints: seas disconnected from the global ocean can produce freshwater imbalance in GCMs and narrow ocean passages require high resolution ocean grids to allow ocean flux calculation (Rosenbloom et al., 2011). Some studies, indeed, suggest that the Tethys passage closure might have played a role in Middle Miocene atmosphere and ocean circulation patterns (Ramstein et al., 1997; Hamon et al., 2013).

AdditionalSome important modifications were applied to the original dataset of Herold et al. (2008) regarding Antarctic ice-sheet geometry, sea-level and configuration of the South East Asian and Panama seawayspassages (see discussion below in subsections 5.1–5.4) (Fig. 3).

5.1 Antarctica

Antarctic ice-sheet geometry was modified for consistency with our ice-sheet volume estimates for the MMCO and MMG (see Sect. 2). In the high southern latitudes, from 60°S to 90°S, the original topography/bathymetry from Herold et al. (2008) was replaced by the Antarctic topography/bathymetry data from David Pollard described above (Fig. 1e,f).

5.2 Sea-level

Sea-level was adjusted to ~48 m and ~5 m above present-day for the MMCO and MMG, respectively (Table 1). These values were derived from our sea-level equivalent estimates (see above) by assuming 64 m of present-day sea-level equivalent. This present-day estimate is in good agreement with Vaughan et al. (2013) (58.3 m for the Antarctic ice-sheet and 7.36 m for the Greenland ice-sheet). The adjustments were applied taking into account that sea-level is ~52 m above present-day in Herold et al. (2008) (Nicholas Herold, pers. comm.) and at present-day level in David Pollard's data. We note that the sea-level adjustment of 4 m (i.e. 48 m above present-day instead of 52 m) with respect toof Herold et al. (2008) for the MMCO is minor and has virtually no effect in common global climate models at low spatial resolution.

5.3 South East Asian gateway

South East Asian paleogeography was modified based on Hall's (2012) reconstruction constrained at 15 Ma (Fig. 43). Hall's data, available as a georeferenced image, were converted into grid format using ArcGIS. Qualitative height/depth values were assigned to the different geographic features: ~2800 m for volcanoes, ~1000 m for highlands, ~250 m for land, ~-22 m for carbonate platforms, ~-200 m for shallow sea, <-4000 m for deep sea, and ~-5500 m for trenches. After embedding the data into the MMCO global dataset, minor manual smoothing was applied at the margins of the embedded region. ~~This reconstruction was available in jpg format as a georeferenced image. The data needed thus to be converted into grid format before they could be embedded into the global topography/bathymetry datasets. We used ArcGIS: https://www.aregis.com/home/index.html for that purpose. Qualitative height/depth values were assigned to the different geographic features described in Hall (2012): ~2800 m for volcanoes, ~1000 m for highlands, ~250 m for land, ~-22 m for carbonate platforms, ~-200 m for shallow sea, <-4000 m for deep sea, and ~-5500 m for trenches. The border regions between the different geographic features were assigned intermediate values, in order to avoid too steep bathymetry gradients that could cause model computational problems. After that, the data were embedded into the MMCO global topography/bathymetry dataset. Further minor manual smoothing was applied at the margins of the embedded region.~~ Here,

shallow bays were removed and single, shallow grid points surrounded by much deeper grid points were deepened to the adjacent depth. In total, these modifications affected ~0.5% of the total number of grid points.

Based on the depth values assigned to the different geographic features in the South East Asia reconstruction, the deepest connection between the Indian and the Pacific Ocean would be only ~200 m deep. This is probably too shallow, since in the Middle Miocene the Indonesian gateway was likely open for both surface and intermediate water (Kuhnt et al., 2004). Deep water passages were therefore added to the MMCO global topography/bathymetry dataset, based on the postulated Middle Miocene ocean paths across the Indonesian archipelago described in Kuhnt et al. (2004) (Fig. 43). The depth values assigned to these passages are shallower than those of the present-day passages (Kuhnt et al., 2004). Based on an educated guess the depths of the two eastern passages were set to 800 m, shallower than that of the present-day eastern Lifamatola (~1940 m) and Timor (~1300–1450 m) passages (Gordon et al., 2003). The northwestern passage was assigned a depth of 1000 m, shallower than that of the present-day northwestern Sangihe Ridge sill (~1350 m) (Gordon et al., 2003). The depth of the southwestern passage was set to 600 m, slightly shallower than that of the present-day southwestern Dewakang sill (680 m) (Gordon et al., 2003). Assigned widths are somewhat arbitrary. The eastern passages were both given a width of ~150 km (~3 grid cells), and the northwestern and southwestern passages a width of ~350 km (~6 grid cells) and ~220 km (~4 grid cells) respectively.

For the MMG, the same South East Asia topography/bathymetry reconstruction was used as for the MMCO after applying a ~43 m sea-level change, in correspondence with our MMCT sea-level fall estimate (see above).

5.4 Panama ~~passage~~seaway

Also the Panama seaway~~passage~~ was modified such that substantial differences exist compared to Herold et al. (2008) original dataset. Montes et al. (2012) suggest a narrow Panama strait already by the Early Miocene, with a width of ~200 km. Therefore, the width of the seaway was set accordingly in our paleogeographic dataset, together with a depth of ~1000 m which reflects Panama sill reconstructions for the Middle Miocene by Duque-Caro (1990).

6 Global vegetation

The current MMCO and MMG global vegetation reconstructions (Fig. 5~~4~~, Sect. 9) were based on Pound et al. (2012), Wolfe (1985) and Morley (2011). The study by Pound et al. (2012) includes global vegetation reconstructions for the Langhian (15.~~69~~7–13.65 Ma) (approximately the end of the MMCO) and the Serravallian (13.65–11.61 Ma) (roughly coincident with the MMG). Wolfe's (1985) study contains an Early Miocene global vegetation reconstruction. The reconstructions from Pound et al. (2012) and Wolfe (1985) are the only Early/Middle Miocene global reconstructions. Morley's (2011) Middle Miocene reconstruction focuses only on the distribution of tropical forests.

The study by Pound et al. (2012), based on paleobotanical evidence from 617 Middle/Late Miocene data locations, constituted the main source of global vegetation data for our MMCO and MMG boundary conditions. Morley's (2011) study added some detail to the current reconstructions in the tropical areas. Wolfe's (1985) Early Miocene data were used in regions where the Middle Miocene reconstructions by Pound et al. (2012) and Morley (2011) had scarce data coverage and also to characterize the vegetation patterns of the main mountain ranges.

The above studies use different nomenclatures to classify the different types of vegetation. Pound et al. (2012) use the BIOME4 classification (Kaplan, 2001), while Wolfe (1985) uses the classification scheme described in Wolfe (1979). Here, we coded the data in the Land Surface Model (LSM) (Bonan, 1996) biome classification scheme. All biome names in this study are in italics, with LSM biome names in addition set in quotation marks. Table 2 shows how the data from Pound et al. (2012), Wolfe (1985) and Morley (2011) were converted into the LSM scheme. However, we note that the correspondence between biomes of different schemes is not always optimal (see notes in Table 2). The *warm-temperate evergreen broadleaf and mixed forest* BIOME4 biome was converted into the LSM scheme as "*warm mixed forest*". The "*warm mixed forest*" LSM biome represents *a mixture of needleleaf evergreen temperate trees and broadleaf deciduous temperate trees, meanwhilethe warm-temperate evergreen broadleaf and mixed forest BIOME4 biome represents either a) temperate broadleaf evergreen trees alone, or b) cool conifer trees mixed with temperate broadleaf evergreen trees, or c) temperate deciduous trees mixed with either temperate broadleaf evergreen trees or cool conifer trees. The conversion is suboptimal because no broadleaf evergreen temperate trees are present in the "warm mixed forest" LSM biome. Nevertheless, the "warm mixed forest"* still constitutes a fair representation of the *warm-temperate evergreen broadleaf and mixed forest* BIOME4 biome. In case a more precise representation in the LSM scheme of the *warm-temperate evergreen broadleaf and mixed forest* BIOME4 biome was required, the LSM scheme could be modified by adding a new biome containing the exact specific plant types present in the *warm-temperate evergreen broadleaf and mixed forest* BIOME4 biome described above (a similar approach is used in Herold et al., 2010). Note also that Table 2 does not contain all the biomes present in the different vegetation schemes, but only the ones effectively used in the current reconstructions. All biome names in the following are italized, with LSM biome names in addition set in quotation marks.

Neither Pound et al. (2012) nor Wolfe (1985) or Morley (2011) provide the data in a gridded format, a requirement for the use in GCMs. According to the geographical coordinates specified in those reconstructions, we merged the data on a 2°x2° latitude/longitude grid for MMCO and MMG, giving preference to the Middle Miocene reconstructions by Pound et al. (2012) and Morley (2011). The Early Miocene reconstruction of Wolfe (1985) was only used at locations where no data are available from the other two reconstructions. An exception are the Alps, Rocky Mountains, Himalayas and Tibetan Plateau, where we used the information from Wolfe (1985). At the regions where the reconstructions from Pound et al. (2012) and Morley (2011) were conflicting with each other, the reconstruction of Pound et al. (2012) was used, except for locations where the latter was less well constrained by proxy information than Morley (2011).

The MMCO and the MMG global vegetation reconstructions presented here solely differ in terms of *"tundra"* distribution on Antarctica (Fig. 54). In both reconstructions *"tundra"* was assigned to the ice-free regions of Antarctica, taking account of the MMCO and MMG ice-sheet geometries (Fig. 1c,d). Assuming the *"tundra"* distribution to be the only difference in terms of vegetation between the MMCO and the MMG is a simplification. Part of the *warm-temperate evergreen broadleaf and mixed forest* (*"warm mixed forest"* in the LSM scheme) present in the middle latitudes during the Langhian was replaced by "cooler and/or drier temperate biomes" during the Serravallian (Pound et al., 2012). This cooling and/or drying trend was observed for example in areas like western North America or Europe (Pound et al., 2012). Additionally, by the Serravallian, in the tropics, some drier biomes than those present there during the Langhian had started to spread (e.g. in South East Asia) (Pound et al., 2012). Nevertheless, the Langhian and Serravallian global vegetation patterns were 'similar' in comparison with the 'markedly different biome pattern of the Tortonian from that of the Serravallian'(see Fig. 5 and Fig. 6 in Pound et al., 2012), which justifies our simplified approach. However, for studies with a specific focus on vegetation-triggered climatic changes across the MMCT, the user could modify our MMG vegetation dataset (LSM scheme) as follows (based on Pound et al., 2012): a) in the mid-latitudes of western North America, the *"warm mixed forest"* between 40-50°N could be partly replaced with *"warm broadleaf deciduous forest"*. Also a *"cool mixed forest"* could be added in the same region at 42°N; b) in Europe, some *"deciduous shrub land"* could be added to the *"warm mixed forest"* in southern France between 42.5-44°N and 6-9°E, and also between 38-47°N and 29-36°E.

We are aware that the Middle Miocene global vegetation reconstructions presented here are rather coarse. Still, we consider it a fair characterization of the MMCO and MMG global vegetation distributions. Grosso modo, the present reconstructions are characterized by *"cool mixed forest"* at high northern latitudes, predominantly *"warm mixed forest"* at middle latitudes, *"tropical broadleaf evergreen forest"* in the tropics, and *"tundra"* in the ice-free regions of Antarctica (Fig. 54). Compared to PI, the vegetation of the Middle Miocene represents a warmer and wetter climate. In the northern hemisphere high latitudes forests are warmer, with no forest tundra or tundra present. The mid-latitudes present warmer and wetter biomes, with e.g. less shrubland-type biomes. The tropics are wetter, with less savanna and less grasses. There is no evidence for neither a desert in northern Africa (Sahara) nor in central Asia. In the southern hemisphere high latitudes tundra is present at the MMCO and disappears after the Antarctic ice-sheet expansion at the MMG (Pound et al., 2012; Bonan et al., 2002). For a higher degree of detail, in GCMs including a dynamic vegetation component, our Middle Miocene vegetation datasets could be used to initialize the vegetation model. Another valid approach would be using the output from an offline vegetation model as boundary condition (e.g., the ones described in Henrot et al., 2017), although here our aim was to provide vegetation boundary conditions based on palaeobotanical data. A detailed discussion of the vegetation patterns we assigned to each region can be found in the Appendix (Sect. 10).

6.1 Europe

The most widespread biome in the middle latitudes of Europe during the Langhian was the *warm-temperate evergreen broadleaf and mixed forest* (*"warm mixed forest"*) (Pound et al., 2012). On the southern and eastern coast of Spain however, drier biomes such as *temperate xerophytic shrubland* (*"evergreen shrub land"*/*"deciduous shrub land"*) or *temperate deciduous broadleaf savanna* (*"deciduous shrub land"*) were present (Pound et al., 2012) (Fig. 4). The vegetation patterns of the Serravallian were similar to those of the Langhian. However, some drying and/or cooling occurred. In east Europe, for example, the data by Pound et al. (2012) indicate the emergence of *temperate deciduous broadleaf savanna* (*"deciduous shrub land"*). These drier and/or cooler biomes developed during the Serravallian were neglected for simplification in the current reconstructions.

Evidence for the Middle Miocene European high northern latitudes (above 60°N) is missing in Pound et al. (2012). This region was painted with *mixed coniferous forest* (*"cool mixed forest"*) (Fig. 4) in the current MMCO and MMG reconstructions based on Wolfe's (1985) Early Miocene data. We also filled the Alpine area with *mixed coniferous forest* (*"cool mixed forest"*) according to Wolfe (1985).

6.2 Asia

The Asian high northern latitudes were assigned *"cool mixed forest"* in the current MMCO and MMG reconstructions (Fig. 4). Pound et al. (2012) suggest *cool-temperate mixed forest* (*"cool mixed forest"*) to have been the dominant biome in the eastern Asian high northern latitudes during the Middle Miocene. No data are provided for the western Asian high northern latitudes in Pound et al. (2012). Wolfe's (1985) reconstruction suggests two different vegetation patterns for the western Asian high northern latitudes during the Early Miocene, corresponding to north and south. For simplification, only the northern pattern, consisting of *mixed coniferous forest* (*"cool mixed forest"*), was considered in the current reconstructions.

The western Asian middle latitudes were filled with *"warm mixed forest"* (Fig. 4). Pound et al. (2012) propose a "south to north drying and cooling trend" for that region during the Middle Miocene, starting with *warm-temperate evergreen broadleaf and mixed forest* (*"warm mixed forest"*) in the southern part and ending with *temperate deciduous broadleaf savanna* (*"deciduous shrub land"*) in the northern part. For simplification, only the *warm-temperate evergreen broadleaf and mixed forest* (*"warm mixed forest"*) was considered in our current MMCO and MMG boundary conditions.

The Himalayas and the Tibetan Plateau were assigned *mixed coniferous forest* (*"cool mixed forest"*) based on Wolfe's (1985) reconstruction.

The eastern Asian middle latitudes were mainly populated by *warm-temperate evergreen broadleaf and mixed forest* (*"warm mixed forest"*) during the Middle Miocene (Pound et al., 2012) (Fig. 4). Along the coast at ~32°N, there was a *tropical evergreen broadleaf forest* (*"tropical broadleaf evergreen forest"*), and west of 111°E a drier region containing biomes such

as *temperate xerophytic shrubland* (*"evergreen shrub land"/"deciduous shrub land"*) (Pound et al., 2012). This drier region was dismissed for simplification in our MMCO and MMG reconstructions.

Tropical evergreen broadleaf forest (*"tropical broadleaf evergreen forest")* was the dominant biome in India and South East Asia during the Middle Miocene (Pound et al., 2012) (Fig. 4).

6.3 Australia and New Zealand

Tropical evergreen broadleaf forest (*"tropical broadleaf evergreen forest")* was present in northeast Australia during the Middle Miocene (Pound et al., 2012) (Fig. 4). Also in the east, but south of 28°S, *warm-temperate evergreen broadleaf and mixed forest* (*"warm mixed forest"*) was present (Pound et al., 2012).

In Pound et al. (2012) the description of Australia is limited to the east side. A line of *megathermal rain forest* (*"tropical broadleaf evergreen forest"*) was assigned along the north coast in the current reconstructions based on Morley's (2011) Middle Miocene data.

Wolfe's (1985) Early Miocene reconstruction suggests the vegetation patterns of east Australia to be also representative for central Australia. Assuming this would still be valid during the Middle Miocene, the *"warm mixed forest"* assigned to east Australia in the current reconstructions, was extended to central Australia.

Wolfe's (1985) data further suggest similar vegetation patterns for west Australia and the southern coast of Spain during the Early Miocene. Assuming this analogy to be still valid during the Middle Miocene, west Australia was filled with "*evergreen shrub land*"/"*deciduous shrub land*", which is the vegetation assigned to the southern coast of Spain in the current MMCO and MMG reconstructions.

Warm-temperate evergreen broadleaf and mixed forest (*"warm mixed forest"*) occupied New Zealand during the Middle Miocene (Pound et al., 2012) (Fig. 4).

6.4 Antarctica

There is evidence for *low- and high-shrub tundra* and *prostrate dwarf-shrub tundra* (*"tundra"*) at the Antarctic margins during the Langhian (Pound et al., 2012). By the Serravallian, practically no vegetation was present on Antarctica (Pound et al., 2012). In the current MMCO and MMG reconstructions *"tundra"* was assigned to the ice free regions, in consistence with the ice-sheet geometries described above (Fig. 4).

6.5 Africa and the Arabian Peninsula

Africa and the Arabian Peninsula have poor data coverage in Pound et al. (2012). Evidence from Pound et al. (2012) for the most northern part of Africa for the Middle Miocene is restricted to one site (in Tunisia), suggesting a *warm-temperate evergreen broadleaf and mixed forest* (*"warm mixed forest"*). That data site was dismissed in our current MMCO and MMG

reconstructions, in view of the inappropriateness to extrapolate data from only one site to the whole surrounding region. Instead, the most northern part of Africa was set to *"evergreen shrub land"/"deciduous shrub land"* (Fig. 4). Wolfe's (1985) Early Miocene reconstruction suggests similar vegetation patterns for that region as for the southern coast of Spain. Assuming these two regions kept similar vegetation patterns also during the Middle Miocene, *"evergreen shrub land"/"deciduous shrub land"*, the vegetation assigned to the southern coast of Spain in the current MMCO and Middle MMG reconstructions, was also assigned to the most northern part of Africa. Also a narrow belt of *megathermal rain forest* (*"tropical broadleaf evergreen forest"*) was set along the northwest coast, in agreement with Morley's (2011) Middle Miocene reconstruction.

Madagascar was assigned *megathermal rain forest* (*"tropical broadleaf evergreen forest"*), following Morley (2011). Also based on Morley's (2011) reconstruction, an area of *megathermal rain forest* (*"tropical broadleaf evergreen forest")* was defined along the south and southeast coast of southern Africa. Pound et al. (2012) suggest that drier tropical biomes, e.g. *tropical savanna* (*"savanna"*), were present close to the southern coast of southern Africa during the Middle Miocene. These drier biomes were dismissed for simplification in our MMCO and MMG boundary conditions.

Still in southern Africa, north of the *"tropical broadleaf evergreen forest"* line, a region of *"warm mixed forest"* was assigned. Wolfe (1985) suggests similar vegetation patterns for that region and for southeast Australia during the Early Miocene. Assuming those two regions kept similar vegetation patterns also during the Middle Miocene, *"warm mixed forest"*, the biome set for southeast Australia in the current MMCO and MMG reconstructions, was also assigned to that region.

The remaining areas of Africa and the Arabian Peninsula were assigned *"tropical broadleaf evergreen forest"*, although we are aware that this is probably too broad for a characterization, as also drier tropical biomes were present. Wolfe (1985) suggests that *tropical rain forest* (*"tropical broadleaf evergreen forest"*) and other drier tropical biomes populated that region during the Early Miocene. Pound et al. (2012) show occurrence of *tropical evergreen broadleaf forest* (*"tropical broadleaf evergreen forest"*) in equatorial Africa during the Middle Miocene, although combined with drier tropical biomes like *tropical deciduous broadleaf forest and woodland* (*"tropical broadleaf deciduous forest"*) or *tropical savanna* (*"savanna"*). On the Arabian Peninsula, a single site indicates *tropical deciduous broadleaf forest and woodland* (*"tropical broadleaf deciduous forest"*) existed in that area during the Langhian (Pound et al., 2012). These drier tropical biomes were dismissed for simplification in our boundary conditions.

6.6 North America and Greenland

During the Middle Miocene, the western North American high latitudes were populated with *cool-temperate mixed forest* (*"cool mixed forest"*) (Pound et al., 2012) (Fig. 4). Evidence for the eastern North American high latitudes is missing in Pound et al. (2012). Wolfe (1985) suggests two different patterns for the eastern North American high latitudes during the

Early Miocene, at ~60°–65°N and north of ~65°N, respectively. For simplification only the most northern pattern, *mixed coniferous forest* (*"cool mixed forest"*), was considered in the current MMCO and MMG reconstructions.

During the Langhian, *warm-temperate evergreen broadleaf and mixed forest* (*"warm mixed forest"*) was prevalent in the western North American middle latitudes above 40°N (Pound et al., 2012). South of 40°N a drier region existed, with biomes such as *temperate xerophytic shrubland* (*"evergreen shrub land"/"deciduous shrub land"*) (Pound et al., 2012) (Fig. 4). During the Serravallian, the western North American middle latitudes became more heterogeneous in terms of vegetation, an amalgam of *warm-temperate evergreen broadleaf and mixed forest* (*"warm mixed forest"*) combined with other drier and/or cooler biomes (Pound et al., 2012). For simplification, the Langhian pattern was used in both MMCO and MMG reconstructions.

The Rocky Mountains were set to *mixed coniferous forest* (*"cool mixed forest"*) following Wolfe (1985).

The central North American middle latitudes were assigned *"warm mixed forest"* in the current MMCO and MMG reconstructions based on Wolfe (1985). That region has scarce data coverage in Pound et al. (2012) (one Langhian site, two Serravallian sites). Wolfe (1985) suggests two different patterns for the central North American middle latitudes during the Early Miocene, corresponding to south and north. For the southern part, Wolfe (1985) suggests similar vegetation patterns as for southeast Australia (assigned *"warm mixed forest"* here), and for the northern part, similar vegetation patterns as for the European middle latitudes (assigned *"warm mixed forest"* here).

However, the central North American middle latitudes were not exclusively vegetated by *"warm mixed forest"* during the Middle Miocene. Wolfe (1985) suggests the presence of "at least some interfluve grassland" in areas such as Nebraska during the late Middle Miocene. Besides, Pound et al. (2012) show some evidence for the presence of *temperate grassland* (*"cool grassland"*) (Langhian) and *temperate deciduous broadleaf savanna* (*"deciduous shrub land"*) (Serravallian) in the central American middle latitudes during the Middle Miocene. These biomes were, however, dismissed for simplification in our current reconstructions.

The eastern North American middle latitudes were also assigned *"warm mixed forest"* in the current MMCO and MMG reconstructions. Pound et al. (2012) suggest *warm-temperate evergreen broadleaf and mixed forest* (*"warm mixed forest"*) existed in eastern North America between 29°N and 39°N, both during the Langhian and the Serravallian. However, outside that interval of latitude no data were available from Pound et al. (2012). Since Wolfe (1985) suggests similar vegetation patterns for the central and eastern North American middle latitudes during the Early Miocene, assuming this analogy would still be valid during the Middle Miocene, *"warm mixed forest"* was also applied to the east, north of 39°N and south of 29°N.

No Middle Miocene data were available for Greenland from Pound et al. (2012). North Greenland was filled with *mixed coniferous forest* (*"cool mixed forest"*) in our current reconstructions based on Wolfe (1985). South Greenland was assigned *"warm mixed forest"*, given its similar latitudinal position and relative geographic proximity with Iceland, where *warm-*

temperate evergreen broadleaf and mixed forest (*"warm mixed forest"*) existed during the Middle Miocene according to Pound et al. (2012).

6.7 Central America and south Mexico

Central America and southern Mexico were assigned *"tropical broadleaf evergreen forest"* (Fig. 4). Morley (2011) suggests *megathermal rain forest* (*"tropical broadleaf evergreen forest"*) populated that region in the Middle Miocene. Pound et al. (2012) suggest that the *tropical evergreen broadleaf forest* (*"tropical broadleaf evergreen forest"*) coexisted with drier tropical biomes (Langhian) and with temperate biomes (Langhian and Serravallian), and proposes altitude as an explanation for the presence of temperate biomes in that region during the Middle Miocene. The drier tropical biomes and the temperate biomes were dismissed in our current MMCO and MMG reconstructions for simplification.

6.8 Northern South America

In northern South America, the northern half and the east were filled with *"tropical broadleaf evergreen forest"* in our reconstructions (Fig. 4). Pound et al. (2012) suggest *tropical evergreen broadleaf forest* (*"tropical broadleaf evergreen forest"*) as the main biome in that region during the Langhian and Serravallian. Nevertheless, they also show evidence for some *tropical deciduous broadleaf forest and woodland* (*"tropical broadleaf deciduous forest"*) in that region during the Serravallian. Morley (2011) suggests the presence of *megathermal rain forest (*"*tropical broadleaf evergreen forest"*) and *monsoonal megathermal forest* (*"tropical broadleaf deciduous forest"*) in that region during the Middle Miocene. The "*tropical broadleaf deciduous forest"* was neglected for simplification in our boundary conditions.

No data were available from Pound et al. (2012) or Morley (2011) for the southwestern part of northern South America. Within that area, the Andes were assigned *"warm mixed forest"* and the rest *"tropical broadleaf evergreen forest"*. For the Early Miocene Andes, Wolfe (1985) suggests similar vegetation patterns as for the most southern part of southern South America. Since significant uplift of the Andes would have started only in the late Miocene (Ghosh et al., 2006), we considered reasonable to assume that these regions kept similar vegetation patterns also during the Middle Miocene. In this way, *"warm mixed forest"*, the biome set in our data for the most southern part of South America (see below), was also assigned to the Andes. Surrounding the Andes there is another area with non-tropical biomes in Wolfe's (1985) reconstruction, which was dismissed here for simplification. The rest of southwest northern South America is occupied by *tropical rain forest* and *paratropical rain forest* (*"tropical broadleaf evergreen forest"*) in Wolfe's (1985) reconstruction.

6.9 Southern South America

During the Middle Miocene, in the northwest of southern South America, there was a region covered by arid biomes such as *temperate xerophytic shrubland* (*"evergreen shrub land"/"deciduous shrub land"*) (Pound et al., 2012) (Fig. 4).

~~In the northeast, along the coast, a narrow belt of *megathermal rain forest* (*"tropical broadleaf evergreen forest"*) was present according to Morley's (2011) Middle Miocene reconstruction.~~

~~No evidence from Pound et al. (2012) or Morley (2011) was available for the area between the arid region in the west and the *"tropical broadleaf evergreen forest"* in the east. East of the arid region, for the area corresponding to the Andes, Wolfe (1985) proposes similar vegetation patterns for the Early Miocene as for the most southern part of southern South America. Assuming these two areas kept similar vegetation patterns also during the Middle Miocene, *"warm mixed forest"*, the biome set in the current MMCO and MMG reconstructions for the most southern part of southern South America (see below), was also assigned to that part of the Andes. For the region east of the Andes, for the Early Miocene, Wolfe (1985) proposes a vegetation pattern similar to that of southeast Australia. Assuming this analogy kept being valid also during the Middle Miocene, *"warm mixed forest"*, the biome set in the current Middle Miocene reconstructions for southeast Australia, was assigned to that region.~~

~~The south of southern South America was filled with *"warm mixed forest"* in our MMCO and MMG reconstructions (Fig. 4). Pound et al. (2012) shows evidence for *warm-temperate evergreen broadleaf and mixed forest* (*"warm mixed forest"*) mixed with *temperate grassland* (*"cool grassland"*) south of 35°S, and again for *warm-temperate evergreen broadleaf and mixed forest* (*"warm mixed forest"*) at 55°S. The *temperate grassland* (*"cool grassland"*) south of 35°S was dismissed here for simplification.~~

7 Testing the boundary conditions with CCSM3

To provide evidence of the suitability of our input data for global climate modeling, we applied the boundary conditions to the Community Climate System Model version 3 (CCSM3). CCSM3 is a fully coupled GCM consisting of components representing atmosphere, ocean, land and sea ice (Collins et al., 2006). A total of three runs were performed: two Miocene runs (MMCO and MMG) and a pre-industrial control run (PI). The atmosphere horizontal grid employed in the PI run, T42, is a Gaussian grid with 64 points in latitude and 128 points in longitude (~2.8° resolution). The notation T42 refers to the spectral truncation level. The land and atmosphere models share the same horizontal grid. The ocean horizontal grid, x1, is a dipole grid with 384 points in latitude and 320 points in longitude. The zonal resolution of the ocean horizontal grid is ~1°, the mean meridional resolution is ~0.5°, refined around the equator (~0.3°). The notation x1 refers to the nominal zonal resolution. The ocean and sea–ice components share the same horizontal grid. The atmosphere and ocean vertical grids have 26 and 40 vertical levels, respectively. This model grid configuration is known as T42x1. ~~For the PI run, the standard configuration T42x1 was used. In that configuration, the atmosphere horizontal grid resolution corresponds to a spectral truncation of T42 (~2.8°). The land and atmosphere models share the same horizontal grid. The horizontal ocean grid is a dipole grid with 384 points in latitude and 320 points in longitude. The zonal resolution is ~1°, the mean meridional resolution is ~0.5°, refined around the equator (~0.3°). The ocean and sea–ice components share the same horizontal grid.~~

~~The atmosphere and ocean vertical grids have 26 and 40 vertical levels, respectively.~~ For the Miocene runs the same grids as for the PI run were used, except for the horizontal ocean (and sea–ice) grid, for which a customized grid was used. This grid is also a dipole grid with 384 points in latitude and 320 points in longitude, although extended to ~87°S (instead of ~79°S) in order to accommodate the changes in the bathymetry off West Antarctica. In the Miocene topography/bathymetry datasets West Antarctica is for the most below sea-level, with ocean reaching down to ~85°S. If the standard CCSM3 grid had been used for the Miocene experiments, the ocean region between ~79°S and 85°S would not have been taken into account in the ocean circulation simulations. The Miocene grid was created from scratch using the CCSM3 setup tools described in Rosenbloom et al. (2011) and it is defined by the following parameters: dyeq=0.25 (meridional grid spacing at the equator, in degrees), dsig=20 (Gaussian e-folding scale at equator), and jcon=45 (rows of constant meridional grid spacing at poles). In some areas the Miocene grid presents a slightly coarser resolution than the PI grid, since both grids have the same number of grid points and the Miocene grid reaches further south than the PI grid. In order to be able to compare the Miocene and PI results, the PI model output data were regridded onto the Miocene grid using the patch recovery method (http://www.ncl.ucar.edu/Applications/ESMF.shtml), which gives better approximations than the bilinear method. We do not think interpolation has any significant effect on the results.

For the PI run, well-mixed greenhouse gases, ozone distribution, aerosols, solar constant and orbital configuration were set to PI following ~~according to~~ Otto-Bliesner et al. (2006). The boundary conditions summarized in Table 1 were used for the Miocene experiments. Well-mixed g~~G~~reenhouse gases, ozone, aerosols, ~~and~~ solar constant and orbital configuration were kept the same as in PI, except for CO_2 (Table 3). ~~The orbital configuration differed from the PI setup. Obliquity was set to 23.24° (mean value for the interval 13-15 Ma), eccentricity to 2.13×10^{-4} (minimum during the last 51 Ma in order to minimize the effect of precession), and precession kept at 102.92° (present-day) (Laskar et al., 2004).~~ The PI experiment was branched from the NCAR CCSM3 1870 CE control run ~~(archived as b30.043)~~ and integrated another 150 years (850 years in total). The Miocene experiments were integrated for a total of 1500 years. The last 100 years of each simulation were used for the analysis. The temperature trends in the deep ocean (at 4-5 km depth) are < 0.14, 0.15, and 0.17 °C/100 years in the PI, MMCO, and MMG cases, respectively. At that same depth range, the salinity trends are <0.01, 0.007, and 0.01 psu/100 years for PI, MMCO, and MMG, respectively. These values represent quasi-equilibrium conditions and we consider them sufficiently small for the focus of this study.

~~Figure 5 shows mean annual precipitation and sea-surface temperature (SST) for the MMCO and MMG simulations relative to the control run.~~ The global mean precipitation rates are 3.00, 2.86, and 2.72 mm/day for the MMCO, MMG, and PI experiments, respectively. Some patterns distinguishing the Miocene runs from the PI run include lower precipitation rates during the Miocene along the northwest coast of South America (15°S-10°N)(up to 3-~~4~~5-~~6~~ mm/day lower)(Fig. 6, Fig. 7), although reaching further inland. In central Africa, between 20°S-5°N, the results show values also up to 3-4 mm/day lower than PI, which might be related to the reduced Miocene east African topography (Jung et al., 2016). ~~In the Indian Ocean, at~~

~~the Bay of Bengal, values up to 4-5 mm/day higher than PI are observed~~. An intensification of the precipitation occurs in the Indian Ocean, compared to PI, with the ITCZ reaching further north at ~90°E (Bay of Bengal). On the contrary, in the equatorial Pacific the PI run exhibits higher precipitation rates than the Miocene runs. These changes in the rainbelt patterns could be related to the different extent and distribution of ice-sheets in both hemispheres. Other studies have already suggested that global ice-sheets might have an effect on the ITCZ (Holbourn et al., 2010; Groeneveld et al., 2017). Other interesting patterns are the ~~The results indicate a~~ decrease in precipitation across the MMCT over the east African coast, between 0-20°N (0.5-2 mm/day lower), as well as the drying at high latitudes (0-1 mm/day). Regarding SSTs (Fig. 6), the highest values correspond to the MMCO experiment, with a mean global SST of 19.62°C, followed by the MMG experiment (18.04°C) and the PI experiment (16.85°C). The decrease in SST across the MMCT is particularly evident in the southern high latitudes and the northern North Pacific (values up to 6-7°C lower). When considering surface air temperatures (at 2 m height), our results show mean global values of 16.38°C, 13.88°C, and 12.16°C for the MMCO, MMG, and PI, respectively (Fig. 8). The modelled decrease in mean global surface air temperatures (2.5°C) and SSTs (1.6°C) between MMCO (CO_2 = 400 ppmv) and MMG (CO_2 = 200 ppmv) is in good agreement with the CCSM3 climate sensitivity values suggested in Kiehl et al. (2006). Our global mean surface air temperature and precipitation values support the idea of a Middle Miocene climate warmer and wetter than PI, and a cooling and drying trend across the MMCT. Mg/Ca data from ODP Hole 1171C on the South Tasman Rise indicate cooling of SSTs of ~2°C across the MMCT (Shevenell et. al, 2004). This value is within our range of cooling estimates for the Southern Ocean. Knorr and Lohmann (2014) MMCT model results show a decrease of 3.1°C in global mean surface air temperature across the MMCT, a value slightly higher than our 2.5°C estimate. -Although CO_2 is lower in the MMG simulation than in the control run, SSTs are higher for MMG than for PI. Potential causes for a MMG climate warmer than PI are the lower extent of ice-sheets (the Antarctic ice-sheet is smaller and the northern Hemisphere free of ice-sheets in the MMG run), and the different vegetation cover (Knorr et al., 2011). However, unambiguously disentangling the effects of each of the different boundary conditions would require performing a series of sensitivity experiments, which is beyond the scope of the current study. Here our aim was testing the idoneity of the current boundary conditions as input data in GCMs for MMCO and MMG experiments.

8 Concluding remarks

The current study describes and provides a complete set~~compilation~~ of boundary conditions for GCMs characterizing the MMCO and the MMG periods. These boundary conditions include global topography, bathymetry and vegetation, and have a particular focus on the Antarctic ice-sheet and the South East Asian gateway. Besides, atmospheric CO_2 concentrations and sea-level estimates were reviewed in detail. Other GCM input data, which strongly depend on the technical details of

individual GCMs, like river routing, were not discussed~~treated~~ here, but can be constructed from the provided topographic datasets.

All data gathered in this study are available in the supplement, ready for use in GCMs. The compilation of boundary conditions for GCMs is time-consuming, especially when referring to deep time periods such as the Miocene. This assemblage of data can be used by the paleomodeling community as a base for a wide variety of Middle Miocene studies, particularly for those related to the MMCT. Output data from two global climate model experiments using these boundary conditions were briefly described here, in order to proof the suitability of the new sets of boundary conditions for modeling purposes.

Despite ongoing efforts, the Middle Miocene is still a period with scarce data availability and thus the Middle Miocene picture presented here is inevitably subject to large uncertainties. More data, improved methods and higher resolutions are required in order to improve the current boundary conditions and hence obtain more detailed and reliable model results.

9 Data availability

All the MMCO and MMG boundary conditions described above, as well as the CCSM3 model output files from the MMCO, MMG, and PI experiments, can be found in NetCDF format in the supplement and at PANGAEA. The MMCO and MMG global topography/bathymetry data are available from the 0.5~~2~~°x0.5~~2~~° lat/lon grid files mmco_topo_bathy_v1_0.nc and mmg_topo_bathy_v1_0.nc, respectively. The MMCO and MMG global vegetation data can be found in the 2°x2° lat/lon grid files mmco_veg_v1_0.nc and mmg_veg_v1_0.nc, respectively. The CCSM3 output files are named MMCO_exp.nc, MMG_exp.nc, and PI_exp.nc, for MMCO, MMG, and PI, respectively.

10 Appendix

10.1 Europe

The most widespread biome in the middle latitudes of Europe during the Langhian was the *warm-temperate evergreen broadleaf and mixed forest* (*"warm mixed forest"*) (Pound et al., 2012). On the southern and eastern coast of Spain however, drier biomes such as *temperate xerophytic shrubland* (*"evergreen shrub land"/"deciduous shrub land"*) or *temperate deciduous broadleaf savanna* (*"deciduous shrub land"*) were present (Pound et al., 2012) (Fig. 5). The vegetation patterns of the Serravallian were similar to those of the Langhian. However, some drying and/or cooling occurred. In east Europe, for example, the data by Pound et al. (2012) indicate the emergence of *temperate deciduous broadleaf savanna* (*"deciduous shrub land"*). These drier and/or cooler biomes developed during the Serravallian were neglected for simplification in the current reconstructions.

Evidence for the Middle Miocene European high northern latitudes (above 60°N) is missing in Pound et al. (2012). This region was painted with *mixed coniferous forest* (*"cool mixed forest"*) (Fig. 5) in the current MMCO and MMG reconstructions based on Wolfe's (1985) Early Miocene data. We also filled the Alpine area with *mixed coniferous forest* (*"cool mixed forest"*) according to Wolfe (1985).

10.2 Asia

The Asian high northern latitudes were assigned *"cool mixed forest"* in the current MMCO and MMG reconstructions (Fig. 5). Pound et al. (2012) suggest *cool-temperate mixed forest* (*"cool mixed forest"*) to have been the dominant biome in the eastern Asian high northern latitudes during the Middle Miocene. No data are provided for the western Asian high northern latitudes in Pound et al. (2012). Wolfe's (1985) reconstruction suggests two different vegetation patterns for the western Asian high northern latitudes during the Early Miocene, corresponding to north and south. For simplification, only the northern pattern, consisting of *mixed coniferous forest* (*"cool mixed forest"*), was considered in the current reconstructions.

The western Asian middle latitudes were filled with *"warm mixed forest"* (Fig. 5). Pound et al. (2012) propose a "south to north drying and cooling trend" for that region during the Middle Miocene, starting with *warm-temperate evergreen broadleaf and mixed forest* (*"warm mixed forest"*) in the southern part and ending with *temperate deciduous broadleaf savanna* (*"deciduous shrub land"*) in the northern part. For simplification, only the *warm-temperate evergreen broadleaf and mixed forest* (*"warm mixed forest"*) was considered in our current MMCO and MMG boundary conditions.

The Himalayas and the Tibetan Plateau were assigned *mixed coniferous forest* (*"cool mixed forest"*) based on Wolfe's (1985) reconstruction.

The eastern Asian middle latitudes were mainly populated by *warm-temperate evergreen broadleaf and mixed forest* (*"warm mixed forest"*) during the Middle Miocene (Pound et al., 2012) (Fig. 5). Along the coast at ~32°N, there was a *tropical evergreen broadleaf forest* (*"tropical broadleaf evergreen forest"*), and west of 111°E a drier region containing biomes such as *temperate xerophytic shrubland* (*"evergreen shrub land"/"deciduous shrub land"*) (Pound et al., 2012). This drier region was dismissed for simplification in our MMCO and MMG reconstructions.

Tropical evergreen broadleaf forest (*"tropical broadleaf evergreen forest"*) was the dominant biome in India and South East Asia during the Middle Miocene (Pound et al., 2012) (Fig. 5).

10.3 Australia and New Zealand

Tropical evergreen broadleaf forest (*"tropical broadleaf evergreen forest"*) was present in northeast Australia during the Middle Miocene (Pound et al., 2012) (Fig. 5). Also in the east, but south of 28°S, *warm-temperate evergreen broadleaf and mixed forest* (*"warm mixed forest"*) was present (Pound et al., 2012).

In Pound et al. (2012) the description of Australia is limited to the east side. A line of *megathermal rain forest* (*"tropical broadleaf evergreen forest"*) was assigned along the north coast in the current reconstructions based on Morley's (2011) Middle Miocene data.

Wolfe's (1985) Early Miocene reconstruction suggests the vegetation patterns of east Australia to be also representative for central Australia. Assuming this would still be valid during the Middle Miocene, the *"warm mixed forest"* assigned to east Australia in the current reconstructions, was extended to central Australia.

Wolfe's (1985) data further suggest similar vegetation patterns for west Australia and the southern coast of Spain during the Early Miocene. Assuming this analogy to be still valid during the Middle Miocene, west Australia was filled with "*evergreen shrub land*"/"*deciduous shrub land*", which is the vegetation assigned to the southern coast of Spain in the current MMCO and MMG reconstructions.

Warm-temperate evergreen broadleaf and mixed forest (*"warm mixed forest"*) occupied New Zealand during the Middle Miocene (Pound et al., 2012) (Fig. 5).

10.4 Antarctica

There is evidence for *low- and high-shrub tundra* and *prostrate dwarf-shrub tundra* (*"tundra"*) at the Antarctic margins during the Langhian (Pound et al., 2012). By the Serravallian, practically no vegetation was present on Antarctica (Pound et al., 2012). In the current MMCO and MMG reconstructions *"tundra"* was assigned to the ice-free regions, in consistence with the ice-sheet geometries described above (Fig. 5).

10.5 Africa and the Arabian Peninsula

Africa and the Arabian Peninsula have poor data coverage in Pound et al. (2012). Evidence from Pound et al. (2012) for the most northern part of Africa for the Middle Miocene is restricted to one site (in Tunisia), suggesting a *warm-temperate evergreen broadleaf and mixed forest* (*"warm mixed forest"*). That data site was dismissed in our current MMCO and MMG reconstructions, in view of the inappropriateness to extrapolate data from only one site to the whole surrounding region. Instead, the most northern part of Africa was set to *"evergreen shrub land"/"deciduous shrub land"* (Fig. 5). Wolfe's (1985) Early Miocene reconstruction suggests similar vegetation patterns for that region as for the southern coast of Spain. Assuming these two regions kept similar vegetation patterns also during the Middle Miocene, *"evergreen shrub land"/"deciduous shrub land"*, the vegetation assigned to the southern coast of Spain in the current MMCO and Middle MMG reconstructions, was also assigned to the most northern part of Africa. Also a narrow belt of *megathermal rain forest* (*"tropical broadleaf evergreen forest"*) was set along the northwest coast, in agreement with Morley's (2011) Middle Miocene reconstruction.

Madagascar was assigned *megathermal rain forest* (*"tropical broadleaf evergreen forest"*), following Morley (2011). Also based on Morley's (2011) reconstruction, an area of *megathermal rain forest* (*"tropical broadleaf evergreen forest")* was defined along the south and southeast coast of southern Africa. Pound et al. (2012) suggest that drier tropical biomes, e.g. *tropical savanna* (*"savanna"*), were present close to the southern coast of southern Africa during the Middle Miocene. These drier biomes were dismissed for simplification in our MMCO and MMG boundary conditions.

Still in southern Africa, north of the *"tropical broadleaf evergreen forest"* line, a region of *"warm mixed forest"* was assigned. Wolfe (1985) suggests similar vegetation patterns for that region and for southeast Australia during the Early Miocene. Assuming those two regions kept similar vegetation patterns also during the Middle Miocene, *"warm mixed forest"*, the biome set for southeast Australia in the current MMCO and MMG reconstructions, was also assigned to that region.

The remaining areas of Africa and the Arabian Peninsula were assigned *"tropical broadleaf evergreen forest"*, although we are aware that this is probably too broad for a characterization, as also drier tropical biomes were present. Wolfe (1985) suggests that *tropical rain forest* (*"tropical broadleaf evergreen forest"*) and other drier tropical biomes populated that region during the Early Miocene. Pound et al. (2012) show occurrence of *tropical evergreen broadleaf forest* (*"tropical broadleaf evergreen forest"*) in equatorial Africa during the Middle Miocene, although combined with drier tropical biomes like *tropical deciduous broadleaf forest and woodland* (*"tropical broadleaf deciduous forest"*) or *tropical savanna* (*"savanna"*). On the Arabian Peninsula, a single site indicates *tropical deciduous broadleaf forest and woodland* (*"tropical broadleaf deciduous forest"*) existed in that area during the Langhian (Pound et al., 2012). These drier tropical biomes were dismissed for simplification in our boundary conditions.

10.6 North America and Greenland

During the Middle Miocene, the western North American high latitudes were populated with *cool-temperate mixed forest* (*"cool mixed forest"*) (Pound et al., 2012) (Fig. 5). Evidence for the eastern North American high latitudes is missing in Pound et al. (2012). Wolfe (1985) suggests two different patterns for the eastern North American high latitudes during the Early Miocene, at ~60°–65°N and north of ~65°N, respectively. For simplification only the most northern pattern, *mixed coniferous forest* (*"cool mixed forest"*), was considered in the current MMCO and MMG reconstructions.

During the Langhian, *warm-temperate evergreen broadleaf and mixed forest* (*"warm mixed forest"*) was prevalent in the western North American middle latitudes above 40°N (Pound et al., 2012). South of 40°N a drier region existed, with biomes such as *temperate xerophytic shrubland* (*"evergreen shrub land"/"deciduous shrub land"*) (Pound et al., 2012) (Fig. 5). During the Serravallian, the western North American middle latitudes became more heterogeneous in terms of vegetation, an amalgam of *warm-temperate evergreen broadleaf and mixed forest* (*"warm mixed forest"*) combined with other drier and/or

cooler biomes (Pound et al., 2012). For simplification, the Langhian pattern was used in both MMCO and MMG reconstructions.

The Rocky Mountains were set to *mixed coniferous forest* (*"cool mixed forest"*) following Wolfe (1985).

The central North American middle latitudes were assigned *"warm mixed forest"* in the current MMCO and MMG reconstructions based on Wolfe (1985). That region has scarce data coverage in Pound et al. (2012) (one Langhian site, two Serravallian sites). Wolfe (1985) suggests two different patterns for the central North American middle latitudes during the Early Miocene, corresponding to south and north. For the southern part, Wolfe (1985) suggests similar vegetation patterns as for southeast Australia (assigned *"warm mixed forest"* here), and for the northern part, similar vegetation patterns as for the European middle latitudes (assigned *"warm mixed forest"* here).

However, the central North American middle latitudes were not exclusively vegetated by *"warm mixed forest"* during the Middle Miocene. Wolfe (1985) suggests the presence of "at least some interfluve grassland" in areas such as Nebraska during the late Middle Miocene. Besides, Pound et al. (2012) show some evidence for the presence of *temperate grassland* (*"cool grassland"*) (Langhian) and *temperate deciduous broadleaf savanna* (*"deciduous shrub land"*) (Serravallian) in the central American middle latitudes during the Middle Miocene. These biomes were, however, dismissed for simplification in our current reconstructions.

The eastern North American middle latitudes were also assigned *"warm mixed forest"* in the current MMCO and MMG reconstructions. Pound et al. (2012) suggest *warm-temperate evergreen broadleaf and mixed forest* (*"warm mixed forest"*) existed in eastern North America between 29°N and 39°N, both during the Langhian and the Serravallian. However, outside that interval of latitude no data were available from Pound et al. (2012). Since Wolfe (1985) suggests similar vegetation patterns for the central and eastern North American middle latitudes during the Early Miocene, assuming this analogy would still be valid during the Middle Miocene, *"warm mixed forest"* was also applied to the east, north of 39°N and south of 29°N.

No Middle Miocene data were available for Greenland from Pound et al. (2012). North Greenland was filled with *mixed coniferous forest* (*"cool mixed forest"*) in our current reconstructions based on Wolfe (1985). South Greenland was assigned *"warm mixed forest"*, given its similar latitudinal position and relative geographic proximity with Iceland, where *warm-temperate evergreen broadleaf and mixed forest* (*"warm mixed forest"*) existed during the Middle Miocene according to Pound et al. (2012).

10.7 Central America and south Mexico

Central America and southern Mexico were assigned *"tropical broadleaf evergreen forest"* (Fig. 5). Morley (2011) suggests *megathermal rain forest* (*"tropical broadleaf evergreen forest"*) populated that region in the Middle Miocene. Pound et al. (2012) suggest that the *tropical evergreen broadleaf forest* (*"tropical broadleaf evergreen forest"*) coexisted with drier

tropical biomes (Langhian) and with temperate biomes (Langhian and Serravallian), and proposes altitude as an explanation for the presence of temperate biomes in that region during the Middle Miocene. The drier tropical biomes and the temperate biomes were dismissed in our current MMCO and MMG reconstructions for simplification.

10.8 Northern South America

In northern South America, the northern half and the east were filled with *"tropical broadleaf evergreen forest"* in our reconstructions (Fig. 5). Pound et al. (2012) suggest *tropical evergreen broadleaf forest* (*"tropical broadleaf evergreen forest"*) as the main biome in that region during the Langhian and Serravallian. Nevertheless, they also show evidence for some *tropical deciduous broadleaf forest and woodland* (*"tropical broadleaf deciduous forest"*) in that region during the Serravallian. Morley (2011) suggests the presence of *megathermal rain forest* (*"tropical broadleaf evergreen forest"*) and *monsoonal megathermal forest* (*"tropical broadleaf deciduous forest"*) in that region during the Middle Miocene. The "*tropical broadleaf deciduous forest"* was neglected for simplification in our boundary conditions.

No data were available from Pound et al. (2012) or Morley (2011) for the southwestern part of northern South America. Within that area, the Andes were assigned *"warm mixed forest"* and the rest *"tropical broadleaf evergreen forest"*. For the Early Miocene Andes, Wolfe (1985) suggests similar vegetation patterns as for the most southern part of southern South America. Since significant uplift of the Andes would have started only in the late Miocene (Ghosh et al., 2006), we considered reasonable to assume that these regions kept similar vegetation patterns also during the Middle Miocene. In this way, *"warm mixed forest"*, the biome set in our data for the most southern part of South America (see below), was also assigned to the Andes. Surrounding the Andes there is another area with non-tropical biomes in Wolfe's (1985) reconstruction, which was dismissed here for simplification. The rest of southwest northern South America is occupied by *tropical rain forest* and *paratropical rain forest* (*"tropical broadleaf evergreen forest"*) in Wolfe's (1985) reconstruction.

10.9 Southern South America

During the Middle Miocene, in the northwest of southern South America, there was a region covered by arid biomes such as *temperate xerophytic shrubland* (*"evergreen shrub land"/"deciduous shrub land"*) (Pound et al., 2012) (Fig. 5).

In the northeast, along the coast, a narrow belt of *megathermal rain forest* (*"tropical broadleaf evergreen forest"*) was present according to Morley's (2011) Middle Miocene reconstruction.

No evidence from Pound et al. (2012) or Morley (2011) was available for the area between the arid region in the west and the *"tropical broadleaf evergreen forest"* in the east. East of the arid region, for the area corresponding to the Andes, Wolfe (1985) proposes similar vegetation patterns for the Early Miocene as for the most southern part of southern South America.

Assuming these two areas kept similar vegetation patterns also during the Middle Miocene, *"warm mixed forest"*, the biome set in the current MMCO and MMG reconstructions for the most southern part of southern South America (see below), was

also assigned to that part of the Andes. For the region east of the Andes, for the Early Miocene, Wolfe (1985) proposes a vegetation pattern similar to that of southeast Australia. Assuming this analogy kept being valid also during the Middle Miocene, *"warm mixed forest"*, the biome set in the current Middle Miocene reconstructions for southeast Australia, was assigned to that region.

The south of southern South America was filled with *"warm mixed forest"* in our MMCO and MMG reconstructions (Fig. 5). Pound et al. (2012) shows evidence for *warm-temperate evergreen broadleaf and mixed forest* (*"warm mixed forest"*) mixed with *temperate grassland* (*"cool grassland"*) south of 35°S, and again for *warm-temperate evergreen broadleaf and mixed forest* (*"warm mixed forest"*) at 55°S. The *temperate grassland* (*"cool grassland"*) south of 35°S was dismissed here for simplification.

Acknowledgements

This research is part of the Marie Curie Initial Training Network Throughflow, funded by the E.U. 7th Framework Programme on Research, Technological Development and Demonstration. The CCSM3 simulations were performed on the Cray XC30/40~~/XC30~~ supercomputer of the Norddeutscher Verbund für Hoch- und Höchstleistungsrechnen (HLRN). We are particularly grateful to Robert Hall, Nicholas Herold, David Pollard and Matthew Pound for their contributions in the assemblage of boundary conditions. We also want to acknowledge Lydie Dupont, Sandra Passchier and Matthew Huber for that. We are grateful to Gary Strand, Sam Levis, Esther Brady, Stephen Yeager, and in particular to Nan Rosenbloom (NCAR) for their help in the model setup procedure. A very special thanks goes to Gabriel Gaus and Lars Nerger (HLRN) for their support in the execution of the model runs. Thanks also to Andreas Manschke for the IT support, to Ute Merkel and Gerlinde Jung for sharing their expertise in CCSM3, ~~and~~ to Hanno Keil for his introduction to ArcGIS, and to Alexandra-Jane Henrot and Petra Langebroek for their constructive reviews that helped to improve the manuscript. We are also grateful to the Throughflow Network, and the Bremen International Graduate School for Marine Sciences GLOMAR.

References

Billups, K. and Schrag, D. P.: Paleotemperatures and ice volume of the past 27 Myr revisited with paired Mg/Ca and $^{18}O/^{16}O$ measurements on benthic foraminifera, Paleoceanography, 17(1), 3–1–3–11, doi:10.1029/2000PA000567, 2002.

Billups, K. and Schrag, D. P.: Application of benthic foraminiferal Mg/Ca ratios to questions of Cenozoic climate change, Earth Planet. Sc. Lett., 209(1–2), 181–195, doi:10.1016/S0012-821X(03)00067-0, 2003.

Bonan, G. B.: A Land Surface Model (LSM Version 1.0) for Ecological, Hydrological, and Atmospheric Studies: Technical Description and User's Guide, NCAR Technical Note NCAR/TN–417+STR, National Center for Atmospheric Research, Boulder, Colorado, 1–150, doi:10.5065/D6DF6P5X, 1996.

Bonan, G. B., Levis, S., Kergoat, L., and Oleson, K.W.: Landscapes as patches of plant functional types: An integrating concept for climate and ecosystem models, Global Biogeochemical Cycles, 16(2), 5-1–5-23, doi:10.1029/2000GB001360, 2002.

Collins, W. D., Bitz, C. M., Blackmon, M. L., Bonan, G. B., Bretherton, C.S., Carton, J. A., Chang, P., Doney, S. C., Hack, J. J., Henderson, T. B., Kiehl, J. T., Large, W. G., McKenna, D. S., Santer, B. D. and Smith, R. D.: The Community Climate System Model Version 3 (CCSM3), J. Clim., 19, 2122–2143, doi:10.1175/JCLI3761.1, 2006.

De Boer, B., Van De Wal, R. S. W., Bintanja, R., Lourens, L. J. and Tuenter, E.: Cenozoic global ice-volume and temperature simulations with 1-D ice-sheet models forced by benthic $\delta^{18}O$ records, Ann. Glaciol., 51(55), 23–33, doi:10.3189/172756410791392736, 2010.

DeConto, R. M., Pollard, D., Wilson, P. A., Paelike, H., Lear, C. H. and Pagani, M.: Thresholds for Cenozoic bipolar glaciation, Nature, 455, 652–656, doi:10.1038/nature07337, 2008.

Duque-Caro, H.: Neogene stratigraphy, paleoceanography and paleobiogeography in northwest South America and the evolution of the Panama seaway, Palaeogeogr. Palaeocl., 77(3–4), 203–234, doi:10.1016/0031-0182(90)90178-A, 1990.

Fairbanks, R. G. and Matthews R. K.: The marine oxygen isotope record in Pleistocene coral, Barbados, West Indies, Quat. Res., 10(2), 181–196, doi:10.1016/0033-5894(78)90100-X, 1978.

Flower, B. P. and Kennett, J. P.: The middle Miocene climatic transition: East Antarctic ice sheet development, deep ocean circulation and global carbon cycling, Palaeogeogr. Palaeocl., 108(3–4), 537–555, doi:10.1016/0031-0182(94)90251-8, 1994.

Foster, G. L., Lear, C. H. and Rae, J. W. B.: The evolution of pCO_2, ice volume and climate during the middle Miocene, Earth Planet. Sc. Lett., 341–344, 243–254, doi:10.1016/j.epsl.2012.06.007, 2012.

Fretwell, P., Pritchard, H. D., Vaughan, D. G., Bamber, J. L., Barrand, N. E., Bell, R., Bianchi, C., et al.: Bedmap2: improved ice bed, surface and thickness datasets for Antarctica, Cryosphere, 7, 375–393, doi:10.5194/tc-7-375-2013, 2013.

Gasson, E., DeConto, R. M., Pollard, D. and Levy, R. H.: Dynamic Antarctic ice sheet during the early to mid-Miocene, P. Natl. Acad. Sci., 113(13), 3459–3464, doi:10.1073/pnas.1516130113, 2016.

Ghosh, P., Garzione, C. N. and Eiler, J. M.: Rapid Uplift of the Altiplano Revealed Through ^{13}C–^{18}O Bonds in Paleosol Carbonates, Science, 311(5760), 511-515, doi: 10.1126/science.1119365, 2006.

Gordon, A. L., Giulivi, C. F. and Ilahude, A. G.: Deep topographic barriers within the Indonesian seas, Deep-Sea Res. II, 50(12–13), 2205–2228, doi:10.1016/S0967-0645(03)00053-5, 2003.

Greenop, R., Foster, G. L., Wilson, P. A. and Lear, C. H.: Middle Miocene climate instability associated with high-amplitude CO_2 variability, Paleoceanography, 29(9), 845–853, doi:10.1002/2014PA002653, 2014.

Groeneveld, J., Henderiks, J., Renema, W., McHugh, C. M., De Vleeschouwer, D., Christensen, B. A., Fulthorpe, C. S., Reuning, L., Gallagher, S. J., Bogus, K., Auer, G., Ishiwa, T., and Expedition 356 Scientists: Australian shelf sediments reveal shifts in Miocene Southern Hemisphere westerlies, Sci. Adv., 3(5), 1–9, doi:10.1126/sciadv.1602567, 2017.

Hall, R: Sundaland and Wallacea: geology, plate tectonics and palaeogeography, in: Biotic Evolution and Environmental Change in Southeast Asia, edited by Gower, D. J., Richardson, J. E., Rosen, B. R., Rueber, L. and Williams, S. T., Cambridge University Press, 32-78, 2012.

Hamon, N., Sepulchre, P., Lefebvre, V. and Ramstein, G.: The role of eastern tethys seaway closure in the middle miocene climatic transition (ca. 14 Ma), Clim. Past, 9(6), 2687–2702, doi:10.5194/cp-9-2687-2013, 2013.

Haq, B. U., Hardenbol, J. and Vail, P. R.: Chronology of Fluctuating Sea Levels Since the Triassic, Science, 235(4793), 1156–1167, doi:10.1126/science.235.4793.1156, 1987.

Henrot, A.-J., Utescher, T., Erdei, B., Dury, M., Hamon, N., Ramstein, G., Krapp, M., Herold, N., Goldner, A., Favre, E., Munhoven, G., and François, L.: Middle Miocene climate and vegetation models and their validation with proxy data, Palaeogeogr. Palaeoclimatol. Palaeoecol., 467, 95–119, doi:10.1016/j.palaeo.2016.05.026, 2017.

Herold, N., Seton, M., Müller, R. D., You, Y. and Huber, M.: Middle Miocene tectonic boundary conditions for use in climate models, Geochem. Geophy. Geosy., 9(10), Q10009, doi:10.1029/2008GC002046, 2008.

Herold, N., Müller, R., and Seton, M.: Comparing early to middle Miocene terrestrial climate simulations with geological data, Geosphere, 6 (6), 952–961, doi:10.1130/GES00544.1, 2010.

Herold, N., Huber, M. and Müller, R. D.: Modeling the miocene climatic optimum. Part I: Land and atmosphere, J. Clim., 24, 6353–6372, doi:10.1175/2011JCLI4035.1, 2011.

Herold, N., Huber, M., Müller, R. D., Seton, M.: Modeling the Miocene climatic optimum: Ocean circulation, Paleoceanography, 27(1), PA1209, doi:10.1029/2010PA002041, 2012.

Holbourn, A., Kuhnt, W., Schulz, M. and Erlenkeuser, H.: Impacts of orbital forcing and atmospheric carbon dioxide on Miocene ice-sheet expansion, Nature, 438(7067), 483–487, doi:10.1038/nature04123, 2005.

Holbourn, A., Kuhnt, W., Schulz, M., Flores, J. A. and Andersen, N.: Orbitally-paced climate evolution during the middle Miocene "Monterey" carbon-isotope excursion, Earth Planet. Sc. Lett., 261(3–4), 534–550, doi:10.1016/j.epsl.2007.07.026, 2007.

Holbourn, A., Kuhnt, W., Regenberg, M., Schulz, M., Mix, A., and Andersen, N.: Does Antarctic glaciation force migration of the tropical rain belt?, Geology, 38(9), 783–786, doi:10.1130/G31043.1, 2010.

John, C. M., Karner, G. D., Browning, E., Leckie, R. M., Mateo, Z., Carson, B. and Lowery, C.: Timing and magnitude of Miocene eustasy derived from the mixed siliciclastic-carbonate stratigraphic record of the northeastern Australian margin, Earth Planet. Sc. Lett., 304(3–4), 455–467, doi:10.1016/j.epsl.2011.02.013, 2011.

Jung, G., Prange, M., Schulz, M.: Influence of topography on tropical African vegetation coverage, Climate Dynamics, 46(7–8), 2535-2549, doi:10.1007/s00382-015-2716-9, 2016.

Kaplan, J. O.: Geophysical Applications of Vegetation Modeling, Ph. D. thesis, Lund University, Lund, 128 pp., 2001.

Kiehl, J. T., Shields, C. A., Hack, J. J., Collins, W. D.: The Climate Sensitivity of the Community Climate System Model Version 3 (CCSM3), J. Climate, 19, 2584–2596, doi:10.1175/JCLI3747.1, 2006.

Knorr, G., Butzin, M., Micheels, A., and Lohmann, G.: A warm Miocene climate at low atmospheric CO2 levels, Geophys. Res. Lett., 38, L20701, 1–5, doi:10.1029/2011GL048873, 2011.

Knorr, G. and Lohmann, G.: Climate warming during Antarctic ice sheet expansion at the Middle Miocene transition, Nature Geoscience, 7(5), 376–381, doi:10.1038/ngeo2119, 2014.

Kominz, M. A., Browning, J. V., Miller, K. G., Sugarman, P. J., Mizintseva, S. and Scotese, C. R.: Late Cretaceous to Miocene sea-level estimates from the New Jersey and Delaware coastal plain coreholes: An error analysis, Basin Research, 20(2), 211–226, doi:10.1111/j.1365-2117.2008.00354.x, 2008.

Krapp, M. and Jungclaus, J. H.: The Middle Miocene climate as modelled in an atmosphere–ocean–biosphere model, Clim. Past, 7(4), 1169–1188, doi:10.5194/cp-7-1169-2011, 2011.

Kuerschner, W. M., Kvacek, Z. and Dilcher, D. L.: The impact of Miocene atmospheric carbon dioxide fluctuations on climate and the evolution of terrestrial ecosystems, P. Natl. Acad. Sci., 105(2), 449–453, doi:10.1073/pnas.0708588105, 2008.

Kuhnt, W., Holbourn, A., Hall, R., Zuvela, M. and Kaese, R.: Neogene history of the Indonesian Throughflow, in: Continent-Ocean Interactions Within East Asia Marginal Seas, edited by Clift, P., Kuhnt, W., Wang, P., Hayes, D., Geophysical Monograph Series, 149, 299–320, doi:10.1029/149GM16, 2004.

Langebroek, P. M., Paul, A. and Schulz, M.: Antarctic ice-sheet response to atmospheric CO_2 and insolation in the Middle Miocene, Clim. Past, 5(4), 633–646, doi:10.5194/cp-5-633-2009, 2009.

Langebroek, P. M., Paul, A. and Schulz, M.: Simulating the sea level imprint on marine oxygen isotope records during the middle Miocene using an ice sheet-climate model, Paleoceanography, 25(4), PA4203, doi:10.1029/2008PA001704, 2010.

Laskar, J., Robutel, P., Joutel, F., Gastineau, M., Correia, A. C. M., Levrard, B.: A long term numerical solution for the insolation quantities of the Earth, 428, 261-285, A&A, doi:10.1051/0004-6361:20041335, 2004.

Lear, C. H., Elderfield, H. and Wilson, P.A.: Cenozoic Deep-Sea Temperatures and Global Ice Volumes from Mg/Ca in Benthic Foraminiferal Calcite, Science, 287(5451), 269–272, doi:10.1126/science.287.5451.269, 2000.

Lear, C. H., Mawbey, E. M. and Rosenthal, Y.: Cenozoic benthic foraminiferal Mg/Ca and Li/Ca records: Toward unlocking temperatures and saturation states, Paleoceanography, 25(4), PA4125, doi:10.1029/2009PA001880, 2010.

Le Brocq, A. M., Payne, A. J., and Vieli, A.: An improved Antarctic dataset for high resolution numerical ice sheet models (ALBMAP v1), Earth Syst. Sci. Data., 2(2), 247-260, doi:10.5194/essd-2-247-2010, 2010.

Levy, R., Harwood, D., Florindo, F., Sangiorgi, F., Tripati, R., von Eynatten, H., Gasson, E., Kuhn, G., Tripati, A., DeConto, R., Fielding, C., Field, B., Golledge, N., McKay, R., Naish, T., Olney, M., Pollard, D., Schouten, S., Talarico, F., Warny, S., Willmott, V., Acton, G., Panter, K., Paulsen, T., Taviani, M. and SMS Science Team: Antarctic ice sheet sensitivity to atmospheric CO_2 variations in the early to mid-Miocene, P. Natl. Acad. Sci., 113(13), 3453–3458, doi:10.1073/pnas.1516030113, 2016.

Lewis, A. R., Marchant, D. R., Ashworth, A. C., Hemming, S. R. and Machlus, M. L.: Major middle Miocene global climate change: Evidence from East Antarctica and the Transantarctic Mountains, Geol. Soc. Am. Bull., 119(11–12), 1449–1461, doi:10.1130/B26134.1, 2007.

Miller, K. G., Fairbanks, R. G. and Mountain, G. S.: Tertiary oxygen isotope synthesis, sea level history, and continental margin erosion, Paleoceanography, 2(1), 1-19, doi:10.1029/PA002i001p00001, 1987.

Montes, C., Cardona, A., McFadden, R., Moron, S. E., Silva, C. A., Restrepo-Moreno, S., Ramirez, D. A., Hoyos, N., Wilson, J., Farris, D., Bayona, G. A., Jaramillo, C. A., Valencia, V., Bryan, J. and Flores, J. A.: Evidence for middle Eocene and younger land emergence in central Panama: Implications for Isthmus closure, Geol. Soc. Am. Bull., 124(5–6), 780–799, doi:10.1130/B30528.1, 2012.

Morley, R. J.: Cretaceous and Tertiary climate change and the past distribution of megathermal rainforests, in: Tropical Rainforest Responses to Climatic Change, Bush, M., Flenley, J., Gosling, W., Springer Praxis Books, Berlin, Heidelberg, 1-34, 2011.

Oerlemans, J.: Correcting the Cenozoic $\delta^{18}O$ deep-sea temperature record for Antarctic ice volume, Palaeogeogr. Palaeocl., 208(3–4), 195–205, doi:10.1016/j.palaeo.2004.03.004, 2004.

Otto-Bliesner, B. L., Tomas, R., Brady, E. C., Ammann, C., Kothavala, Z., and Clauzet, G.: Climate sensitivity of moderate and low resolution versions of CCSM3 to preindustrial forcings, J. Climate, 19, 2567–2583, doi:10.1175/JCLI3754.1, 2006.

Pagani, M., Zachos, J. C., Freeman, K. H., Tipple, B., Bohaty, S.: Marked Decline in Atmospheric Carbon Dioxide Concentrations During the Paleogene, Science, 309(5734), 600–603, doi:10.1126/science.1110063, 2005.

Pearson, P. N. and Palmer, M. R.: Atmospheric carbon dioxide concentrations over the past 60 million years, Nature, 406(6797), 695–699, doi:10.1038/35021000, 2000.

Pollard, D.: A retrospective look at coupled ice sheet–climate modeling, Clim. Change, 100, 173-194, doi:10.1007/s10584-010-9830-9, 2010.

Pollard, D. and DeConto, R. M.: Description of a hybrid ice sheet-shelf model, and application to Antarctica, Geosci. Model Dev., 5, 1273-1295, doi:10.5194/gmd-5-1273-2012, 2012

Pound, M. J., Haywood, A. M., Salzmann, U. and Riding, J. B.: Global vegetation dynamics and latitudinal temperature gradients during the Mid to Late Miocene (15.97–5.33Ma), Earth-Sci. Rev., 112(1–2), 1–22, doi:10.1016/j.earscirev.2012.02.005, 2012.

Ramstein, G., Fluteau, F., Besse, J. and Joussaume, S.: Effect of orogeny, plate motion and land-sea distribution on Eurasian climate change over the past 30 million years, Nature, 386, 788-795, doi:10.1038/386788a0, 1997.

Retallack, G. J.: Refining a pedogenic-carbonate CO_2 paleobarometer to quantify a middle Miocene greenhouse spike, Palaeogeogr. Palaeocl., 281(1–2), 57–65, doi:10.1016/j.palaeo.2009.07.011, 2009.

Rögl, F.: Mediterranean and Paratethys. Facts and hypotheses of an Oligocene to Miocene paleogeography (short overview), Geologica carpathica, 50(4), 339–349, 1999.

Rosenbloom, N., Shields, C., Brady, E., Levis, S. and Yeager, S.: Using CCSM3 for Paleoclimate Applications, NCAR Technical Note NCAR/TN–483+STR, National Center for Atmospheric Research, Boulder, Colorado, 1–81, doi:10.5065/D69S1P09, 2011.

Shevenell, A. E., Kennett, J. P., Lea, D.W.: Middle Miocene Southern Ocean Cooling and Antarctic Cryosphere Expansion, Science, 305(5691), 1766-1770, doi:10.1126/science.1100061, 2004.

Shevenell, A. E., Kennett, J. P. and Lea, D. W.: Middle Miocene ice sheet dynamics, deep-sea temperatures, and carbon cycling: A Southern Ocean perspective, Geochem. Geophy. Geosy., 9(2), Q02006, doi:10.1029/2007GC001736, 2008.

Thiede, J., Jessen, C., Knutz, P., Kuijpers, A., Mikkelsen, N., Nørgaard-Pedersen, N. and Spielhagen, R. F.: Millions of Years of Greenland Ice Sheet History Recorded in Ocean Sediments, Polarforschung, 80(3), 141–159, 2011.

Tong, J. A., You, Y., Müller, R. D. and Seton, M.: Climate model sensitivity to atmospheric CO_2 concentrations for the middle Miocene, Glob. Planet. Change, 67(3–4), 129–140, doi:10.1016/j.gloplacha.2009.02.001, 2009.

Tripati, A. K., Roberts, C. D. and Eagle, R. A.: Coupling of CO_2 and Ice Sheet Stability Over Major Climate Transitions of the Last 20 Million Years, Science, 326(5958), 1394–1397, doi:10.1126/science.1178296, 2009.

Vaughan, D. G., Comiso, J. C., Allison, I., Carrasco, J., Kaser, G., Kwok, R., Mote, P., Murray, T., Paul, F., Ren, J., Rignot, E., Solomina, O., Steffen, K., and Zhang, T.: Observations: Cryosphere, in: Climate Change 2013: The Physical Science Basis. Contribution of Working Group I to the Fifth Assessment Report of the Intergovernmental Panel on Climate Change, edited by Stocker, T. F., Qin, D., Plattner, G. K., Tignor, M., Allen, S.

K., Boschung, J., Nauels, A., Xia, Y., Bex, V., and Midgley, P. M., Cambridge University Press, Cambridge, United Kingdom and New York, NY, USA, 317-382, 2013.

Wolfe, J. A.: Temperature parameters of humid to mesic forests of Eastern Asia and relation to forests of other regions of the Northern Hemisphere and Australasia, U.S. Geological Survey professional paper, 1106, 1–37, 1979.

Wolfe, J.A.: Distribution of major vegetational types during the Tertiary, in: The carbon cycle and atmospheric CO_2: natural variations Archean to present, edited by: Sundquist E. T. and Broecker W. S., American Geophysical Union Monograph, 32, 357–375, doi:10.1029/GM032p0357, 1985.

You, Y., Huber, M., Müller, R. D., Poulsen, C. J. and Ribbe, J.: Simulation of the middle miocene climate optimum, Geophys. Res. Lett., 36(4), L04702, doi:10.1029/2008GL036571, 2009.

Zachos, J., Pagani, M., Sloan, L., Thomas, E., Billups, K.: Trends, Rhythms, and Aberrations in Global Climate 65 Ma to Present, Science, 292(5517), 686–693, doi:10.1126/science.1059412, 2001.

Zachos, J. C., Dickens, G. R. and Zeebe, R. E.: An early Cenozoic perspective on greenhouse warming and carbon-cycle dynamics, Nature, 451(7176), 279–283, doi:10.1038/nature06588, 2008.

Zhang, Y. G., Pagani, M., Liu, Z., Bohaty, S. M. and DeConto, R.: A 40-million-year history of atmospheric CO_2, Philos. Trans. R. Soc. A, 371(2001), 20130096, doi:10.1098/rsta.2013.0096, 2013.

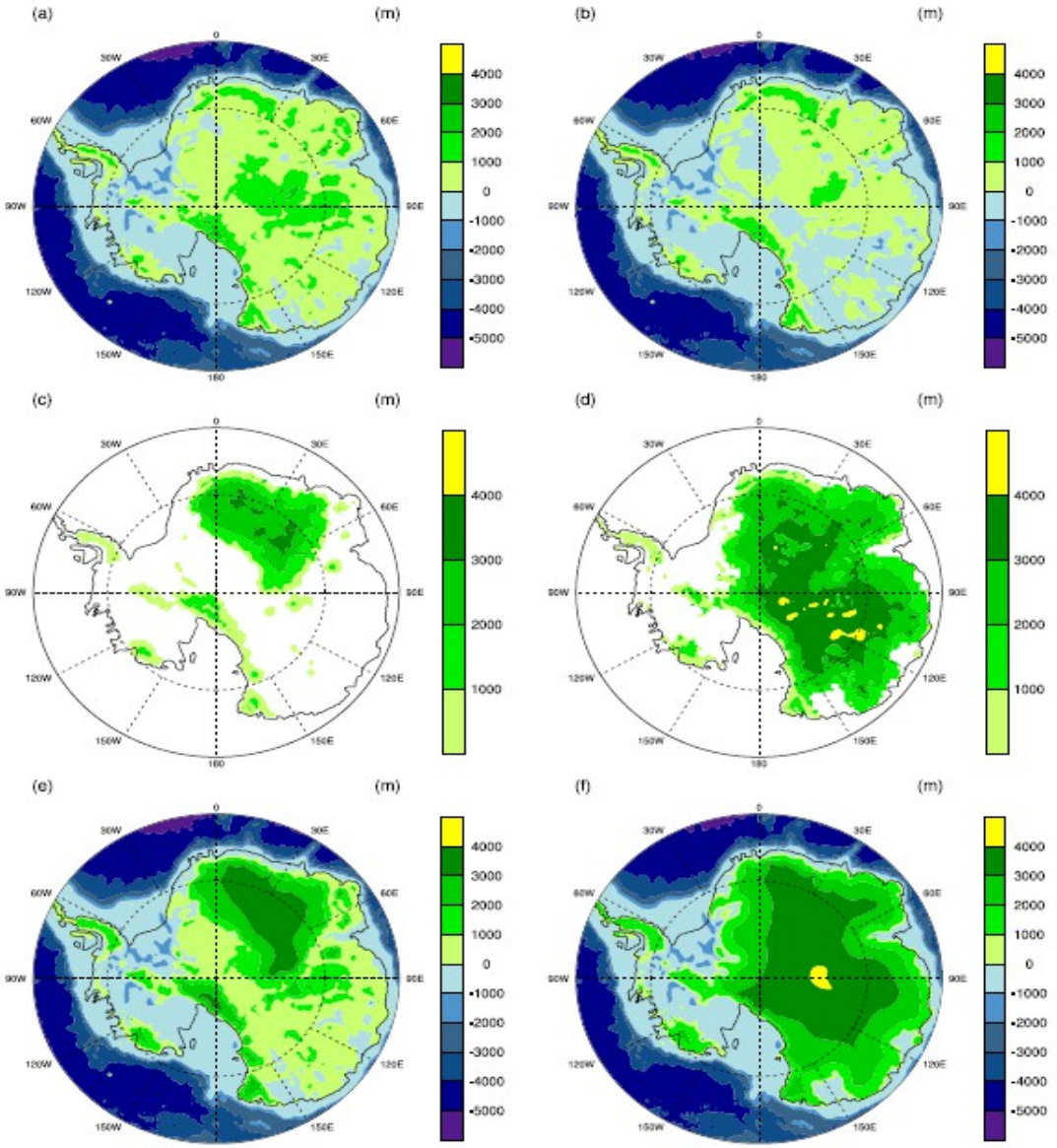

980

Figure 1: Reconstruction of Antarctica for the Middle Miocene Climatic Optimum (MMCO) and the Middle Miocene Glaciation (MMG): (a), (b) bedrock elevation; (c), (d) ice thickness; (e), (f) surface~~total~~ elevation (bedrock elevation + ice thickness), in meters. Black lines represent present day coastline. Data from David Pollard.

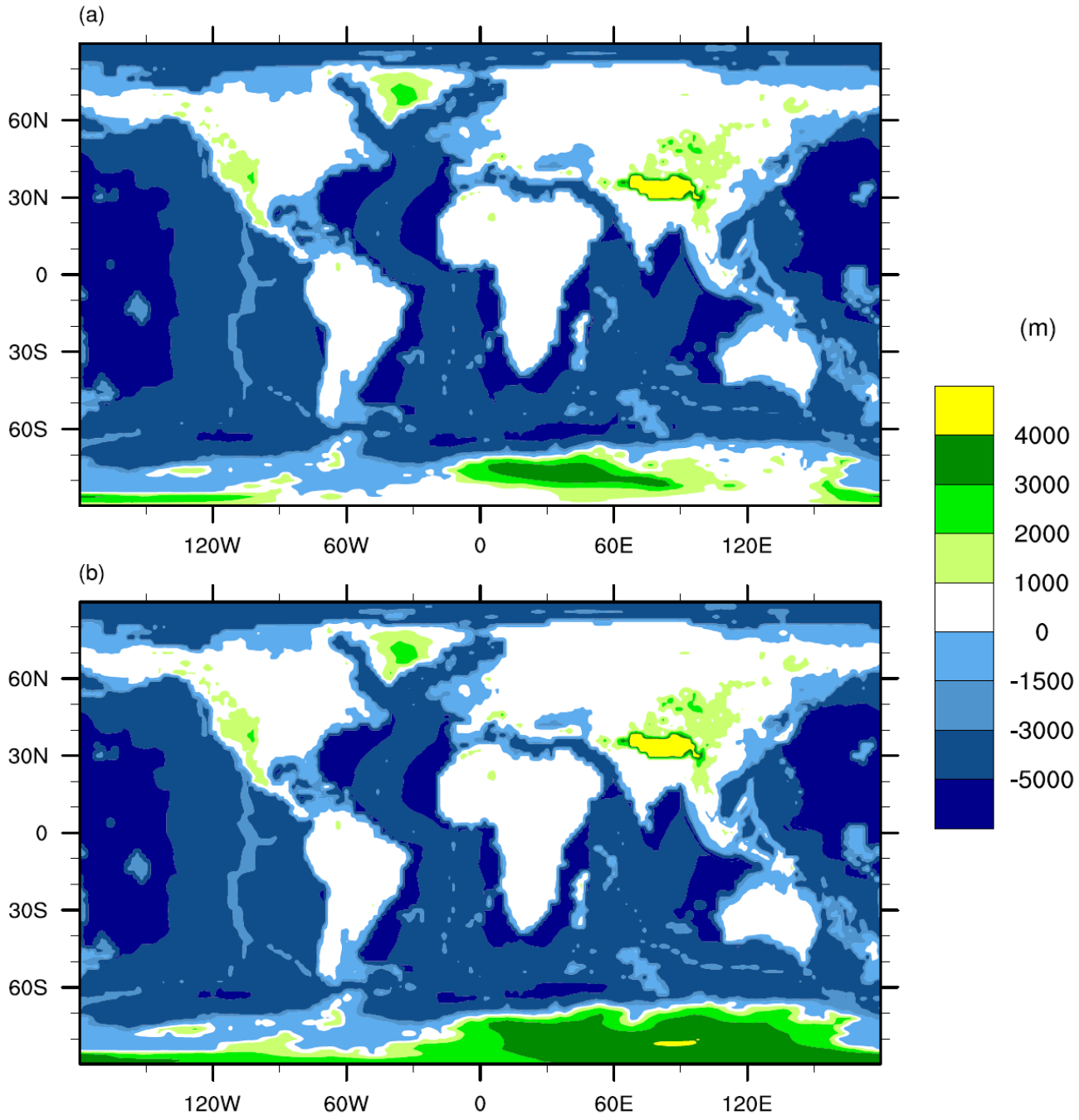

Figure 2: Topography/bathymetry reconstruction for the (a) MMCO and the (b) MMG.

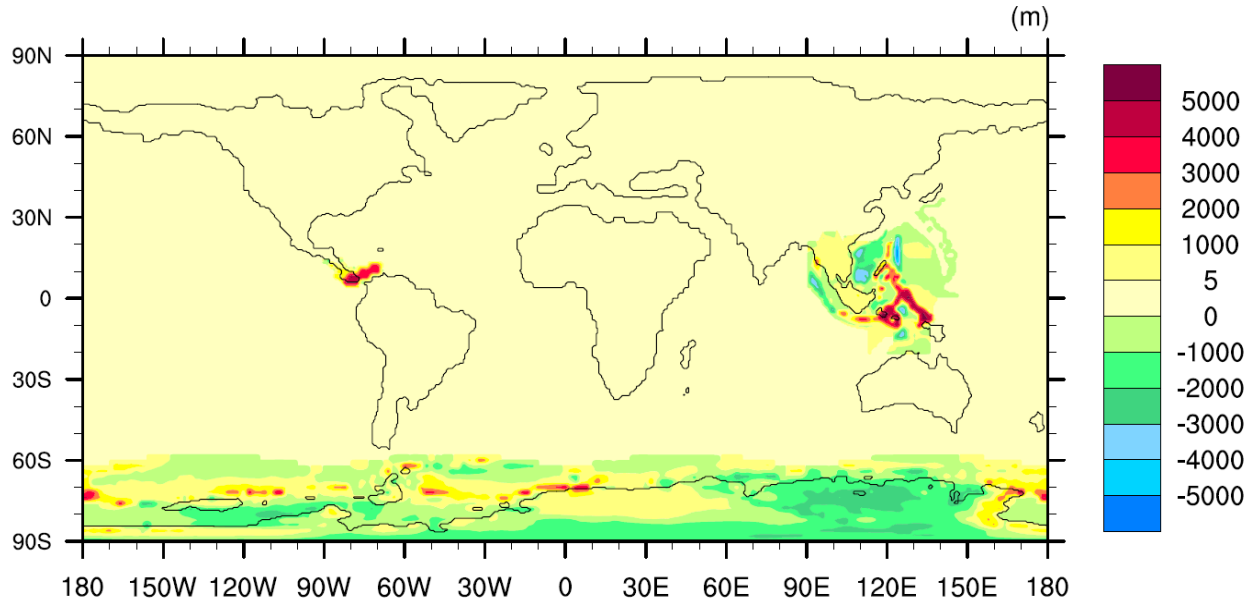

985 **Figure 3: Difference between MMCO and the topography/bathymetry by Herold et al. (2008), in meters. Sea level is 4 m higher in the MMCO dataset (subsection 5.2), the Indonesian Throughflow barriers are shallower (subsection 5.3), the Panama seaway is narrower (subsection 5.4), and the Antarctic topography/bathymetry is based on David Pollard's data (subsection 5.1) and consistent with MMCO ice volume estimates.**

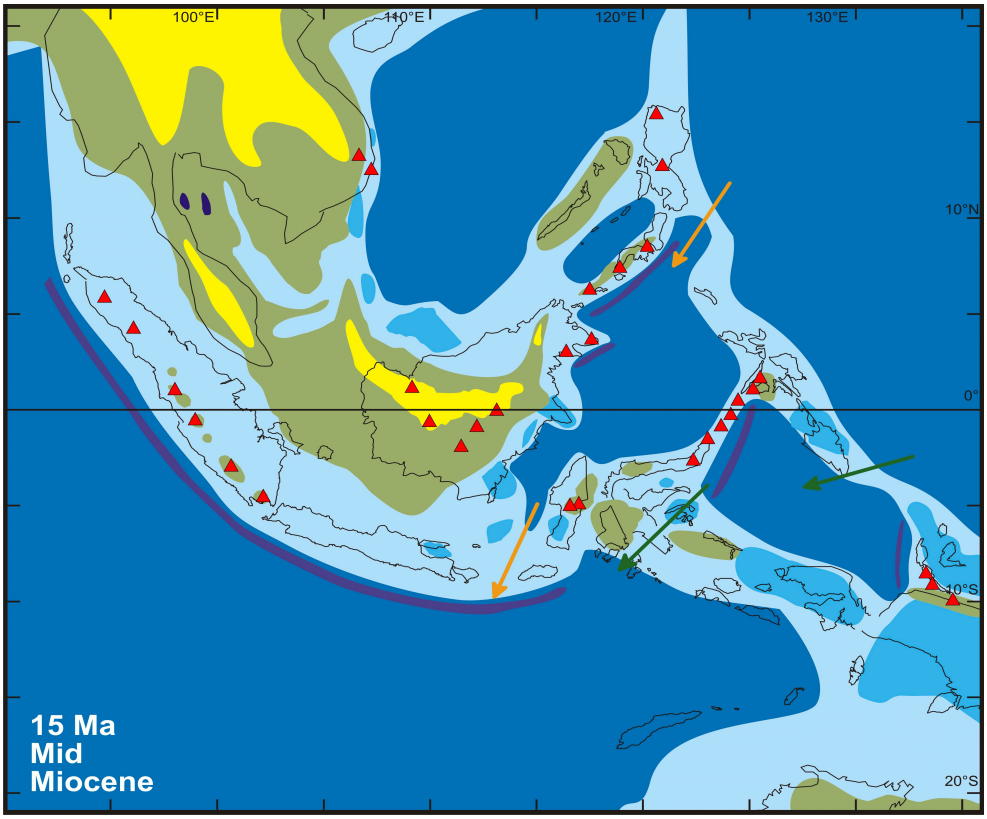

Figure 4: Paleogeographic reconstruction of South East Asia for 15 Ma from Hall (2012). Geographic features: volcanoes in red (triangles), highlands in yellow, land in green, carbonate platforms in blue, shallow sea in light blue, deep sea in dark blue, trenches in violet. Figure courtesy of Robert Hall (Royal Holloway, University of London). Arrows represent Middle Miocene postulated ocean paths across the Indonesian archipelago and are based on Kuhnt et al. (2004). Eastern paths shown in green, western paths in orange.

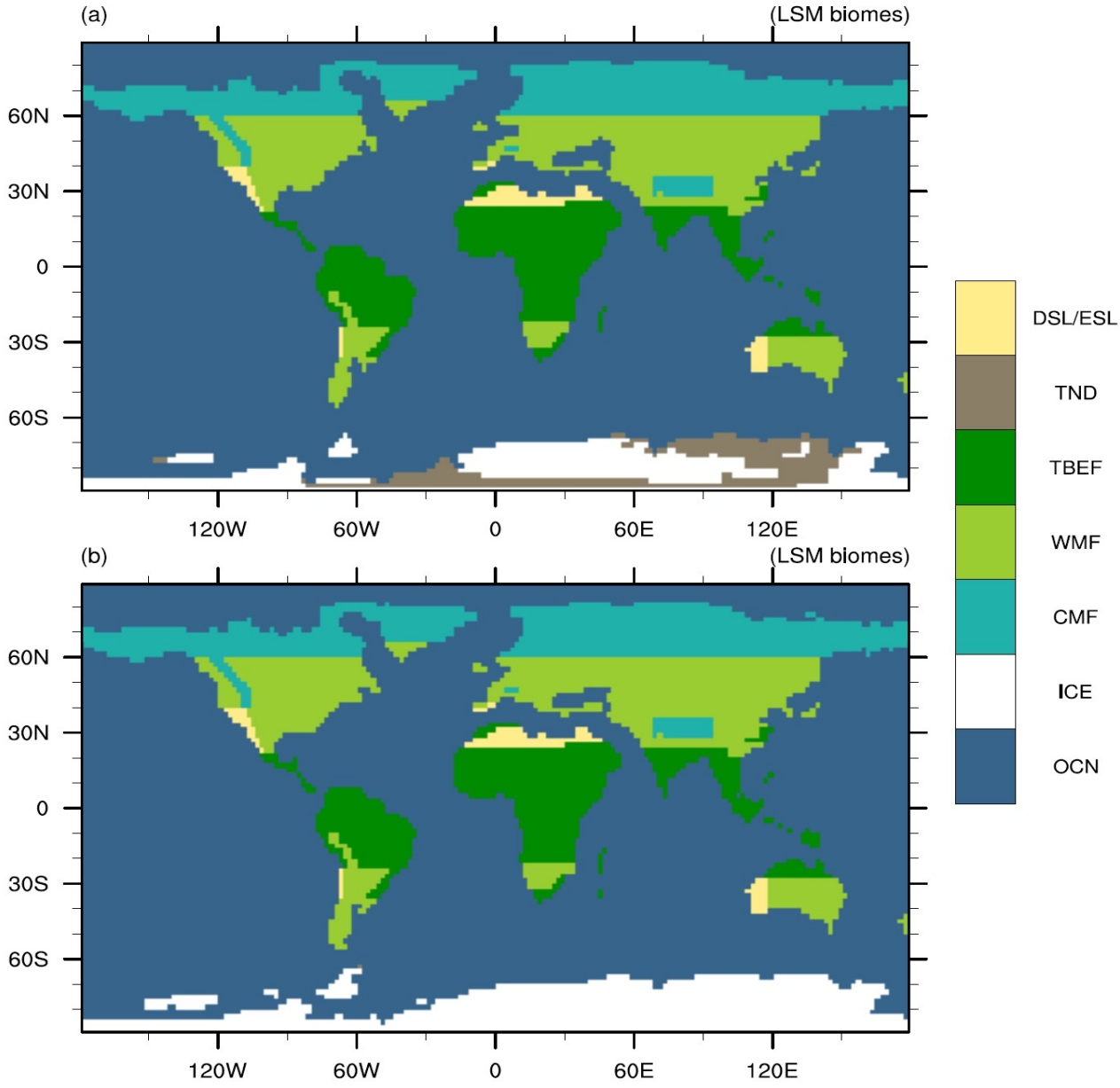

995 **Figure 5: Vegetation reconstruction for the (a) MMCO and the (b) MMG. Colors represent LSM biomes: DSL = deciduous shrubland, ESL = evergreen shrubland, TND = tundra, TBEF = tropical broadleaf evergreen forest, WMF = warm mixed forest,**

CMF = cool mixed forest, ~~WMF = warm mixed forest, TBEF = tropical broadleaf evergreen forest, TND = tundra, ESL = evergreen shrubland, DSL = deciduous shrubland,~~ ICE = land ice, OCN = ocean.

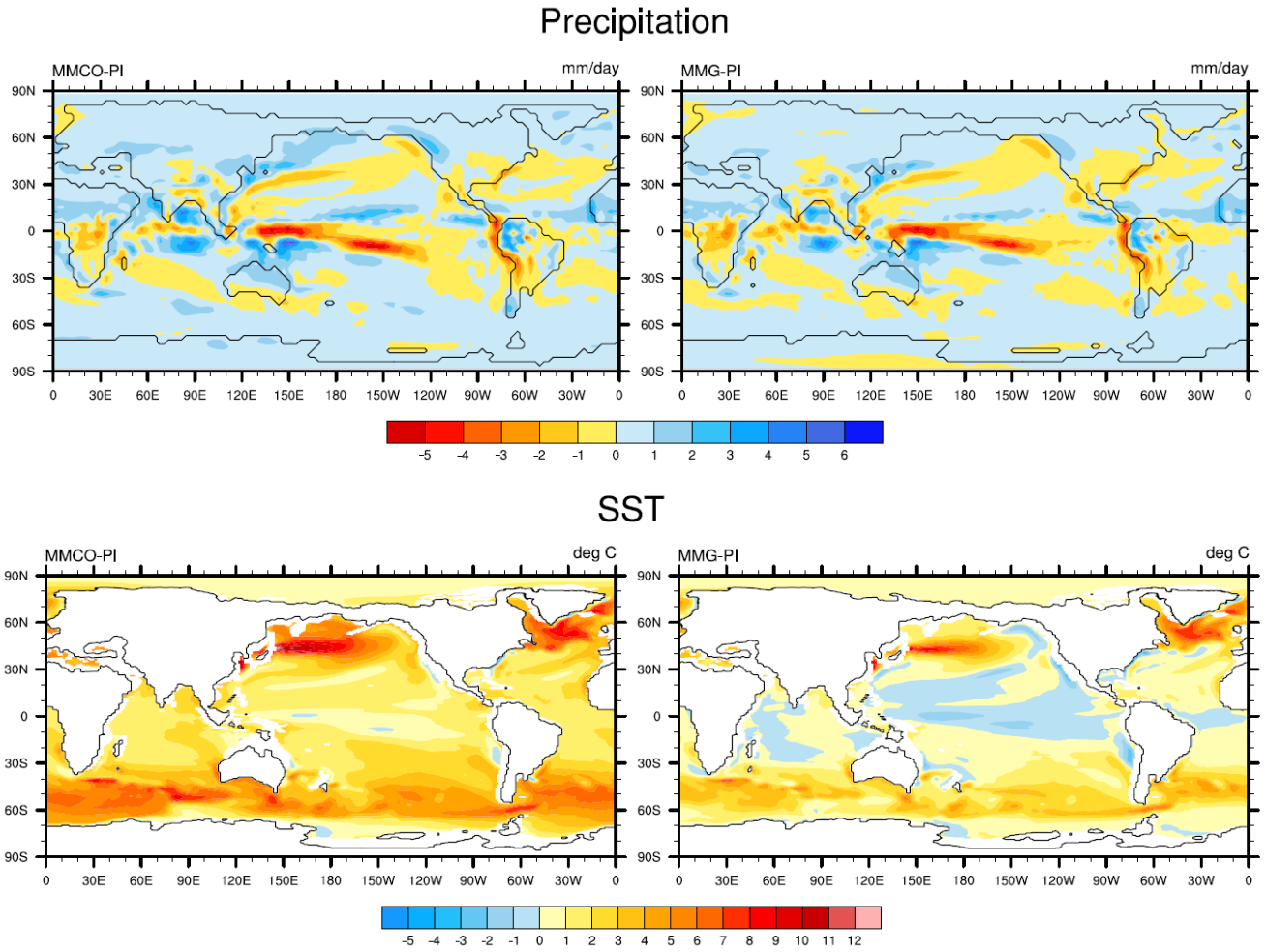

Figure 6: Sea-surface temperature (SST) (°C) and precipitation (in mm/day) differences between MMCO and MMG experiments, and PI, respectively.

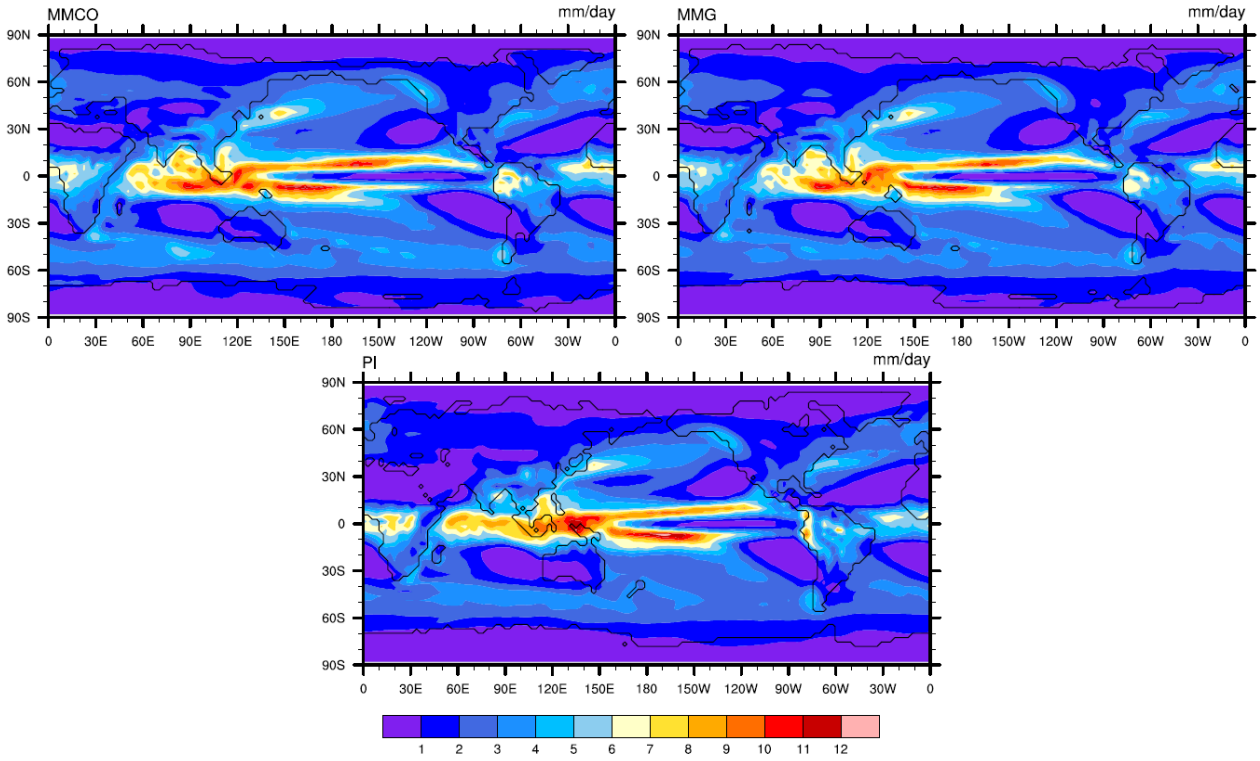

Figure 7: Precipitation for MMCO, MMG, and PI, in mm/day.

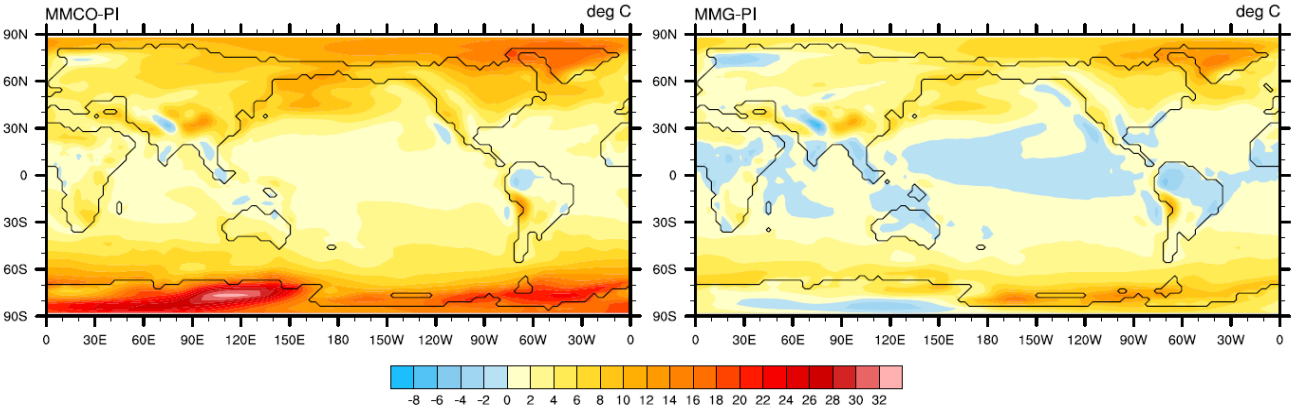

Figure 8: Surface air temperature (at 2 m height) (°C) differences between MMCO and MMG experiments, and PI, respectively.

	MMCO	MMG
Antarctic ice-sheet volume	6 million km³	23 million km³
Sea-level	48 m higher than at present-day	5 m higher than at present-day
Atmospheric CO_2 concentration	400 ppmv	200 ppmv
Global topography/bathymetry	mainly Herold et al. (2008) with modifications for tropical seaways (Hall, 2012; Montes et al., 2012) and the Antarctic ice-sheet	same as MMCO, but with global sea-level reduced by 43 m and an expanded Antarctic ice-sheet
Global vegetation	mainly Pound et al. (2012) with gaps filled according to Wolfe (1985) and Morley (2011); ice and tundra in Antarctica	same as MMCO, but with tundra removed in Antarctica

Table 1: **Summary of boundary conditions for the Middle Miocene Climatic Optimum (MMCO) and the Middle Miocene Glaciation (MMG).**

BIOME4	**LSM**
tropical evergreen broadleaf forest	tropical broadleaf evergreen forest
tropical deciduous broadleaf forest and woodland	tropical broadleaf deciduous forest
warm-temperate evergreen broadleaf and mixed forest	warm mixed forest[1]
cool-temperate mixed forest	cool mixed forest[2]
tropical savanna	savanna
temperate xerophytic shrubland	evergreen shrub land or deciduous shrub land
temperate deciduous broadleaf savanna	deciduous shrub land
temperate grassland	cool grassland
low- and high-shrub tundra	tundra
prostrate dwarf-shrub tundra	tundra
ice	land ice
Wolfe's (1979) classification	**LSM**
mixed coniferous forest	cool mixed forest[3]
tropical rain forest	tropical broadleaf evergreen forest
paratropical rain forest	tropical broadleaf evergreen forest[4]
Morley's (2011) classification	**LSM**
megathermal rain forest	tropical broadleaf evergreen forest
monsoonal megathermal forest	tropical broadleaf deciduous forest

Table 2: **Conversion of vegetation types to the LSM vegetation scheme.**

[1] The *warm-temperate evergreen broadleaf and mixed forest* may contain broadleaf evergreen trees, needleleaf evergreen trees and deciduous trees. The *warm mixed forest* contains needleleaf evergreen trees and deciduous trees, but not broadleaf evergreen trees. [2] The deciduous trees in the *cool-temperate mixed forest* are temperate, meanwhile the ones in the *cool mixed forest* are boreal. [3] The *mixed coniferous forest* is mainly needleleaf evergreen, but broadleaf trees are also present. These can be deciduous or evergreen. The *cool mixed forest* is formed by needleleaf evergreens and broadleaf deciduous. Broadleaf evergreens are not present. [4] The *paratropical rain forest* is mainly broadleaf evergreen, but it may contain some broadleaf deciduous and conifers.

Experiment	PI	MMCO	MMG
CO_2	280 ppmv	400 ppmv	200 ppmv
CH_4	760 ppbv	same as PI	
N_2O	270 ppbv		
CFC's	0		
O_3	1870 A.D.		
Sulfate aerosols	1870 A.D.		
Dust and sea salt	PD		
Carbonaceous aerosols	30% of PD		
Solar constant	1365 Wm^{-2}		
Eccentricity	0.016724		
Obliquity	23.446 °		
Precession	102.04 °		

Table 3: Summary of atmospheric compositiongreenhouse gases, aerosols, solar constant, and orbital configuration for the CCSM3 test experiments. PI values are according to Otto-Bliesner et al. (2006). The orbital configuration represents 1950 A.D. values. PD = present day.